International Journal of Hydrogen Energy 87 (2024) 966–984

Contents lists available at ScienceDirect

International Journal of Hydrogen Energy

journal homepage: www.elsevier.com/locate/he

Investigation on the hydrogen storage properties, electronic, elastic, and thermodynamic of Zintl Phase Hydrides XGaSiH (X = sr, ca, ba)

H. Ammi [a,b], Z. Charifi [c,d,*], H. Baaziz [c,d,**], T. Ghellab [c,d], L. Bouhdjer [a,b], S. Adalla [a,b], H.Y. Ocak [e], Ş. Uğur [f], G. Uğur [f]

[a] Department of Physics, Faculty of Sciences and Applied Sciences, University of Bouira, 10000 Bouira, Algeria
[b] Laboratory of Material Physics and Optoelectronic Compounds, University of Bouira, Algeria
[c] Department of Physics, Faculty of Science, University of M'sila, 28000 M'sila, Algeria
[d] Laboratory of Physics and Chemistry of Materials, University of M'sila, Algeria
[e] Marmara University, Department of Physics Education, 34722 Istanbul, Turkey
[f] Department of Physics, Faculty of Science, Gazi University, 06500 Ankara, Turkey

ARTICLE INFO

Handling Editor: Dr M Mahdi Najafpour

Keywords:
Zintl phase hydrides
Hydrogen storage
Elastic constants
Quasi-harmonic debye model

ABSTRACT

This study presents a comprehensive investigation of the electronic, mechanical, and thermodynamic properties of Zintl phase hydrides XGaSiH (X = Sr, Ca, Ba) using Density Functional Theory (DFT) and the FP-LAPW method within the WIEN2k package. Our analysis covers the structural stability, electronic properties, and hydrogen interaction mechanisms in these compounds. The hydrides exhibit narrow band gaps, with values ranging from 0.1 to 0.5 eV using GGA and LDA functionals, and 0.6–1.0 eV with mBJ-GGA and mBJ-LDA. The hydrogen storage capacities are determined to be 0.34 wt %, 0.47 wt %, and 0.40 wt % for SrGaSiH, CaGaSiH, and BaGaSiH, respectively, highlighting their potential for energy storage applications. Thermodynamic properties, evaluated through the quasi-harmonic Debye model, provide insights into the Grüneisen parameter, heat capacity, and thermal expansion coefficient over a range of pressures (0–50 GPa) and temperatures (up to 1000 K). Elastic constants reveal that these compounds are mechanically stable, with a notable anisotropy in the {100} plane and varying degrees of compressibility among the different hydrides. Our study further highlights the slightly ordered hexagonal Ga and Si layers, which contribute to the enhanced hydrogen storage capabilities of these materials. The compounds demonstrate high structural stability, facilitating effective hydrogen retention and release at practical temperatures, making them promising candidates for hydrogen storage applications. Additionally, the analysis of electronic band structures and density of states suggests significant conductivity potential, with band gaps ranging from 0.1 to 1.0 eV, depending on the computational method used. The unique combination of structural, electronic, thermodynamic, and mechanical properties in XGaSiH compounds positions them as valuable materials for renewable energy applications. These findings lay the groundwork for future research focused on optimizing these materials through structural modifications or doping to enhance performance metrics such as hydrogen storage capacity and electrical conductivity.

1. Introduction

In recent years, there has been an increased demand for research in sustainable and renewable energy sources due to growing concerns about the depletion of traditional fossil fuels such as oil, coal, and gasoline [1]. The consumption of these resources has led to harmful environmental impacts, such as greenhouse gas emissions and climate change, prompting the global community to seek cleaner and more sustainable energy alternatives. In this context, hydrogen energy has emerged as a pivotal solution due to its high abundance, energy content, and sustainability [2]. When used as a fuel, hydrogen produces only water as a byproduct, making it an environmentally friendly option.

Parallel to the growing interest in renewable energy, hydrogen storage technologies have become a major focus due to their critical role in advancing the transition to sustainable energy sources. Among these technologies, electrochemical hydrogen storage methods have emerged

* Corresponding author. Department of Physics, Faculty of Science, University of M'sila, 28000 M'sila, Algeria.
** Corresponding author. Department of Physics, Faculty of Science, University of M'sila, 28000 M'sila, Algeria.
E-mail addresses: charifizoulikha@gmail.com, zoulikha.charifi@univ-msila.dz (Z. Charifi), baaziz_hakim@yahoo.fr, hakim.baaziz@univ-msila.dz (H. Baaziz).

https://doi.org/10.1016/j.ijhydene.2024.09.087
Received 30 July 2024; Received in revised form 5 September 2024; Accepted 6 September 2024
Available online 12 September 2024

as promising solutions, offering moderate storage conditions and the ability to meet sustainable storage needs. For instance, CaGaSiH and SrGaSiH, while exhibiting modest hydrogen storage capacities of 0.47% and 0.34% wt%, respectively, are notable for their stable structural properties and ability to release hydrogen efficiently at suitable desorption temperatures [3]. Additionally, perovskite-based materials show significant potential for developing efficient hydrogen storage systems, thanks to their unique structural and electronic properties [4].

Improving hydrogen storage materials requires innovative strategies based on advanced simulation methods such as the phase-field method, which has proven effective in guiding the design of new materials and enhancing their properties [5]. With recent advancements in energy storage technologies, it has become essential to integrate hydrogen storage systems with other storage systems, such as calcium-ion batteries, to improve overall performance and reduce costs [6]. These efforts involve a comprehensive approach aimed at enhancing the efficiency and safety of hydrogen storage systems by utilizing materials with large surface areas and active conductive properties, thereby improving their hydrogen storage capabilities [7].

Zintl phases serve as a blueprint for designing new solid compounds with multifunctional properties. Named in honor of the German chemist Eduard Zintl, who first studied a subset of intermetallic compounds in the 1930s, these phases consist of positively charged metals combined with elements from groups 13 to 15. Unlike typical intermetallic compounds, Zintl phases exhibit a blend of ionic and covalent bonding and are usually semiconductors. They offer a range of both equivalent and nonequivalent exchanges that uniquely contribute to their properties. Zintl's electron counting rules can be used to predict structural types and establish a foundation for structure-property relationships [8,9].

Although storing hydrogen gas by compressing it in tanks has proven effective, this method has shown limitations in efficiency over prolonged operation periods. The challenges associated with high-pressure hydrogen storage include energy losses during compression, safety concerns, and the need for robust storage infrastructure. As a result, research has increasingly turned to solid-state hydrogen storage methods, which offer superior gravimetric and volumetric energy densities [10]. Among solid-state hydrogen storage systems, metal hydrides and complex hydrides have garnered considerable attention due to their ability to reversibly store and release hydrogen through chemical processes.

Recent studies have expanded the understanding of various hydride materials, such as XVH3 and YCrH3, focusing on their structural, mechanical, and hydrogen storage properties [11,12]. For instance, the gravimetric hydrogen storage capacities of $NaVH_3$, KVH_3, $RbVH_3$, and $CsVH_3$ have been reported to be 3.78, 3.15, 2.12, and 1.59 wt%, respectively, demonstrating the potential of these materials in hydrogen storage applications [11]. Similarly, the hydrides $CaCrH_3$, $SrCrH_3$, and $BaCrH_3$ have shown capacities of 3.08, 2.08, and 1.55 wt%, respectively, further contributing to the body of research focused on hydrogen storage solutions [12].

Complex hydrides like XGaSiH (where X = Sr, Ca, and Ba) show promising potential for hydrogen storage due to their ability to form hydrogen-based conduction bands, enhancing their optoelectronic properties [13]. Understanding the physical properties of XGaSiH hydrides is essential for the advancement of innovative hydrogen storage compounds and solar materials. While some studies have investigated the structural and electronic properties of SrGaSiH, comprehensive information on their thermodynamic and elastic properties, as well as their potential applications in photovoltaics, remains scarce.

This study, titled "Investigation on the Hydrogen Storage Properties, Electronic, Elastic, and Thermodynamic Properties of Zintl Phase Hydrides XGaSiH (X = Sr, Ca, Ba)," is motivated by the need to advance hydrogen storage technologies and better understand the materials that could support this goal. Efficient hydrogen storage is essential for the practical use of hydrogen as a clean energy source, and improving these materials involves not only enhancing their hydrogen storage capacities but also understanding their mechanical stability and elasticity. Zintl phase hydrides, specifically XGaSiH (X = Sr, Ca, Ba), present promising characteristics for hydrogen storage due to their potential high storage capacities and favorable thermodynamic properties. However, their practical application also depends on their mechanical stability, which is crucial for ensuring their durability and performance. By investigating the elastic properties of these hydrides, we aim to assess their mechanical stability and how it relates to their hydrogen storage capabilities. This comprehensive approach provides a valuable contribution to the development of robust and efficient hydrogen storage materials, supporting the broader goal of sustainable energy technologies and their practical implementation.

This study, in Section 2, details the computational methodology employed using Density Functional Theory (DFT) to investigate the hydrides XGaSiH (X = Sr, Ca, and Ba). The analysis encompasses ground state properties, crystal structures, bonding characteristics, and electronic properties such as band structures and density of states (DOS). Thermodynamic properties, including entropy, thermal expansion, and specific heats, are computed via Gibbs energy non-equilibrium methods. Additionally, elastic constants, bulk modulus, and estimated melting temperatures are examined to approximate decomposition behaviors under varying conditions. The study also explores elastic anisotropy and Debye temperatures, providing comprehensive insights into the potential applications of these hydrides for hydrogen storage and energy-related endeavors. Section 4 summarizes the key findings discussed in the conclusion.

2. Details of computation

Section 2 employed the Full Potential Linearized Augmented Plane Wave (FP-LAPW) approach, which was implemented using the WIEN2k code [14]. In order to consider the influence of exchange and correlation effects, the computations utilized the Local Density Approximation (LDA) and the Generalized Gradient Approximation (GGA) [15].

The wave functions in the interstitial area were increased by utilizing plane waves. The cutoff value for these plane waves was set at $k_{max} \times$ R.M.T = 8.0, where R.M.T denotes the radius of the Muffin-Tin sphere. The charge density was increased using a Fourier series up to $G_{max} = 16$ $(Ryd)^{1/2}$, and the valence wave functions within Muffin-Tin spheres were expanded up to $l_{max} = 12$. The energy gap between the core and valence states was defined as −6.0 Ry for these computations. Convergence was attained by applying a self-consistent total energy threshold of 10^{-4} Ry. This was accomplished by using 600 k-points to sample the first Brillouin zone (BZ).

Given that our system lacks partially filled *d* or *f* orbitals crucial for strong bonding interactions, the Hubbard correction (GGA + U) was not applicable. The study employed a DFT-based formalism at absolute zero temperature and pressure, incorporating the (PV) term to account for pressure effects. Temperature effects were considered through thermal contributions to the crystal's free energy. These computational approaches provide essential insights for optimizing production processes and predicting material behavior across varying environmental conditions.

The Gibbs2 code, created by Blanco et al. [16,17], utilises the quasi-harmonic Debye framework [18] to calculate extensive thermodynamic characteristics of materials, specifically considering temperature effects that are not taken into account by the Born-Oppenheimer technique. This computational tool utilises established thermodynamic equations to determine important parameters, including the Debye temperature (θ_D) and the out-of-equilibrium Gibbs function, G*(V, P, T). The Gibbs function in a state of non-equilibrium is mathematically represented as:

$$G^*(x, V; P, T) = E_{sta}(x, V) + PV + F^*_{vib}(x, V; T) + F^*_{el}(x, V; T) \quad (1)$$

Here, x represents a pertinent system parameter such as composition or concentration, and V denotes the system volume. $E_{sta}(x, V)$

encompasses static energy contributions, including those from chemical composition and structural arrangement. The term PV accounts for mechanical work done against external pressure P during volume changes V. The vibrational term $F^*_{vib}(x,V;T)$ represents the contribution from thermal vibrations, while $F^*_{el}(x,V;T)$ captures electronic contributions, such as electronic excitations and interactions between electrons and the crystal lattice.

In this context, V signifies the system volume, while x represents a relevant system parameter, such as concentration or composition. Static energy contributions, such as those resulting from chemical formula and structural arrangement, are included in $E_{sta}(x,V)$. The term "PV" refers to the mechanical labour that is performed regarding external pressure P during changes in volume V. The electronic contributions, including electronic excitations and interactions between electrons and the crystal lattice, are captured by the term $F^*_{el}(x,V;T)$, while the vibrational term $F^*_{vib}(x,V;T)$ represents the contribution from thermal vibrations. For semiconductors like XGaSiH (X = Sr, Ca, Ba), electronic contributions to the Helmholtz free energy are negligible due to fully occupied electron bands.

Equation (1) offers a complete framework for defining non-equilibrium Gibbs free energy under different settings by incorporating these components. The Gibbs function is minimised by expressing it as:

$$G^*(P,T) = \min_{x,V} G^*(x,V;P,T) \tag{2}$$

Minimizing the Gibbs function with respect to volume V can be expressed as:

$$\frac{\delta G^*}{\delta V} = 0 = -P_{sta} + P - P_{th} \tag{3}$$

Here, $P_{sta} = \partial E_{sta}/\partial V$ represents the static pressure, and $P_{th} = \partial F^*_{vib}/\partial V$ denotes the thermal pressure. Solving equation (2) provides the thermal equation of state (EOS). The vibrational energy F^*_{vib} is characterised by the vibrational state density g (ω) in the quasi-harmonic approximation.

$$F^*_{vib} = \int_0^\infty \left[\frac{\omega}{2} + k_B T\right) \ln\left(1 - e^{-\omega/K_B T}\right)\Big] g(\omega)\partial\omega \tag{4}$$

$$F^*(x,V;T) = E_{sta}(x,V) + F^*(x,V;T) \tag{5}$$

The Debye model [19], a widely used approximation for phonon spectra, simplifies the solid as a continuous, isotropic elastic medium. In this model, acoustic waves propagate without dispersion, with frequencies directly proportional to the wave vector $\boldsymbol{k}$. The model condenses the $3p$ phonon branches (where p is the number of basis atoms per unit cell) into three acoustic branches characterized by $\omega = C_D\boldsymbol{k}$, where C_D represents the sound velocity. The total number of vibration modes is $3pN$, where N is the number of primitive unit cells. As a result, the phonon density of states follows a quadratic relationship:

$$g_{Debye}(\omega) = \begin{cases} 9n\omega^2/\omega_D^3 & si\ \omega < \omega_D \\ 0 & si\ \omega \geq \omega_D \end{cases} \tag{6}$$

Here, n represents unit cell density, and ω_D is the Debye frequency correlated with Debye temperature:

$$\theta_D = \frac{\omega_D}{K_B} = \frac{1}{K_B}\left(\frac{6\pi^2 n}{V}\right)^{\frac{1}{3}} \upsilon_0 \tag{7}$$

Where υ_0 represents the average velocity of the three acoustic phonon branches. In the Debye model, the Grüneisen coefficient γ is given by:

$$\gamma = -\frac{\partial \ln \theta_D}{\partial \ln V} \tag{8}$$

Thermodynamic properties determined from gDebye(ω) encompass the Helmholtz free energy (F), entropy (S), heat capacities (specifically C_V and C_p, and the coefficient of thermal expansion (α):

$$F = E_{sta}(x,V) + \frac{9}{8} n K_B \theta_D + 3nK_B T \ln\left(1 - e^{-\theta_D/T}\right) - nK_B T D\left(\frac{\theta_D}{T}\right) \tag{9}$$

$$S = -3nK_B \ln\left(1 - e^{-\theta_D/T}\right) + 4nK_B D\left(\frac{\theta_D}{T}\right) \tag{10}$$

$$C_V = 12nK_B D\left(\theta_D/T\right) - \frac{9nK_B\theta_D/T}{e^{\theta_D/T} - 1} \tag{11}$$

$$C_p = C_v(1 + \alpha\gamma T) \tag{12}$$

$$\alpha = -\frac{1}{V}\left(\frac{\partial V}{\partial T}\right)_p = \frac{\gamma C_V}{B_T V} \tag{13}$$

Here, B_T represents the isothermal compressibility modulus, n denotes the number of atoms per cell, and D(x) denotes the Debye integral:

$$D(x) = \frac{3}{x^3}\int_0^x \frac{y^3 e^y}{1 - e^y}\partial y \tag{14}$$

Elastic constants, crucial for understanding material stability and mechanical behavior, were rigorously determined using the IRELAST method [20] implemented within the WIEN2k package. This computational approach involves applying small strains to the crystal lattice and calculating the resulting stress tensors. By analyzing how the stress responds to strain, elastic constants such as bulk modulus, shear modulus, and Young's modulus were accurately derived. These constants provide fundamental insights into the material's resistance to deformation under external forces and its ability to transmit mechanical energy. The computational framework ensures precision in characterizing the mechanical properties of XGaSiH (X = Sr, Ca, Ba) hydrides, thereby facilitating their potential applications in various technological fields.

3. Results and discussion

3.1. Structural properties

In the exploration of materials suitable for hydrogen storage, a variety of compounds within the AB_2H_2 series have been studied extensively. Compounds such as $SrAl_2H_2$, $BaGa_2H_2$, and $SrGa_2H_2$ have been observed experimentally, demonstrating promising hydrogen storage capacities and stable structural properties. However, other compounds like $BaAl_2H_2$ remain undiscovered. This study hypothesizes that $BaAl_2H_2$ may adopt a structure similar to its counterparts in the series, typically stabilizing in a hexagonal $P3m1$ space group. In this structure, B atoms form puckered graphitic layers surrounded by three nearest A neighbors, with hydrogen filling the remaining coordination sites [21,22].

Departing from traditional oxidation models in chemical entities, Zintl phases offer intriguing deviations where more electronegative elements act as anions, forming polyanions. These Zintl phases, characterized by their electron-precise polyanionic frameworks balanced by metal cations, provide a unique approach to material design. The AeTrTt compounds (Ae = Ca, Sr, Ba; Tr = Al, Ga; Tt = Si, Ge, Sn) represent such a family. Upon hydrogenation, these compounds transform into polar semiconductors, exhibiting band gaps ranging from 0.3 to 0.8 electron volts [15–20,23]. These hydrogenated compounds present exciting

possibilities for various applications, including optoelectronic devices and solar energy systems. Their calculated shift current response surpasses that of $BiFeO_3$ by up to eight times and shows significant responses even at low photon energies, making them potential candidates for next-generation photovoltaic devices. With band gaps below 1 electron volt and some members exhibiting stability in air up to 770 K, these compounds may find utility in solar cell devices, offering a potential alternative to traditional pn-junction solar cells [13]. Their favorable electronic properties, combined with their stability and high hydrogen content, position them as strong candidates for practical hydrogen storage solutions.

The bonding in this group of compounds has been elucidated in two ways: one posits a formal valence state configuration of $(Ae)^{2+}[TrTtH]^{2-}$ or $[AeTrTt]^{1+}(H^{-})$, as discussed in Refs. [22,24,25]. The first model strictly adheres to the Zintl concept, portraying a layered polyanion composed of "three-bonded [Tr-H]$^{-}$" and three-bonded lone electron pair Tt^{-} [25]. This model emphasizes the formal charge separation and the formation of stable polyanionic structures. Conversely, a recent study presents an alternative view, indicating through band structure analysis that H orbital contributions primarily occur approximately 5 eV below the Fermi level, with minor interaction with Tr and Tt bands closer to the *Fermi* level [24]. This perspective suggests a more delocalized bonding scenario, where hydrogen's role is less about forming distinct anionic units and more about contributing to the overall electronic structure.

Understanding these bonding characteristics is crucial for predicting the behavior and stability of these compounds under various conditions. This study aims to provide a comprehensive analysis of the electronic, structural, and thermodynamic properties of these materials, leveraging advanced computational techniques to predict their potential for practical hydrogen storage applications.

Building on the understanding of complex hydrides, this study focuses on the crystalline structure of XGaSiH materials, where X represents Sr (Strontium), Ca (Calcium), and Ba (Barium). These materials are anticipated to adopt hexagonal structures, akin to those observed in the AB_2H_2 series, such as $SrAl_2H_2$ and $BaGa_2H_2$. The hexagonal lattice arrangement of XGaSiH compounds is expected to exhibit unique electronic and bonding characteristics that could influence their hydrogen storage capabilities.

In the AB_2H_2 series, the hexagonal *P*3*m*1 structure facilitates the formation of puckered graphitic layers of B atoms surrounded by their nearest A neighbors, with hydrogen occupying the remaining coordination sites [21,22]. Similarly, XGaSiH materials are predicted to stabilize in a hexagonal lattice, which may lead to comparable bonding environments and electronic properties. Investigating the structural properties of these hydrides will provide deeper insights into their potential for hydrogen storage applications.

The study will explore various aspects of the XGaSiH crystalline structure, including the arrangement of metal and hydrogen atoms, the stability of the hexagonal lattice, and the influence of different metal cations (Sr, Ca, Ba) on the overall structure. By examining these factors, the research aims to elucidate how the specific arrangement of atoms affects the hydrogen storage capacity and stability of these materials. Understanding the structural characteristics of XGaSiH compounds is crucial for optimizing their performance in hydrogen storage applications. The insights gained from this study will contribute to the development of advanced hydrogen storage materials with improved efficiency and practicality, aligning with ongoing efforts to advance sustainable and renewable energy technologies.

The hexagonal phase of XGaSiH materials, specifically in the *P*3*m*1 space group (*No. 156*), has been thoroughly investigated, as illustrated in Fig. 1. This phase aligns with theoretical predictions made by Vajeeston et al. [26] and John et al. [13], which forecasted that XGaSiH compounds would crystallize in a hexagonal structure at lower temperatures (see Table 1).

To determine the stability and energetics of this phase, total energy calculations were performed by varying the unit cell volume and analyzing the results using the Murnaghan equation of state [27]. Fig. 2 presents the relationship between total energy and volume, calculated using both the Local Density Approximation (LDA) and the Generalized Gradient Approximation (GGA). The study also measured the equilibrium lattice constants a, b, and c, as well as the bulk modulus *B* and its pressure derivative B', for the XGaSiH (X = Sr, Ca, Ba) compounds. These results are detailed in Table 2 and show strong agreement with data from previous investigations [26].

Notably, the XGaSiH compounds exhibit a discernible trend of decreasing bulk modulus from CaGaSiH to SrGaSiH to BaGaSiH. The unit cell volumes, calculated using GGA and LDA approximations, show a progressive increase: from 66.73 $Å^3$ to 72.62 $Å^3$ to 80.23 $Å^3$ (GGA) and from 64.39 $Å^3$ to 70.31 $Å^3$ to 78.05 $Å^3$ (LDA) as the structure transitions from CaGaSiH to SrGaSiH and ultimately to BaGaSiH. The volume discrepancies calculated using the GGA approximation compared to values reported by Michael J. and colleagues [28] are 2.76%, 2.30%, and 3.72% for SrGaSiH, CaGaSiH, and BaGaSiH, respectively.

These findings underscore the accuracy of the theoretical models and highlight the systematic variation in structural properties across the XGaSiH series. The observed patterns provide valuable insights into the

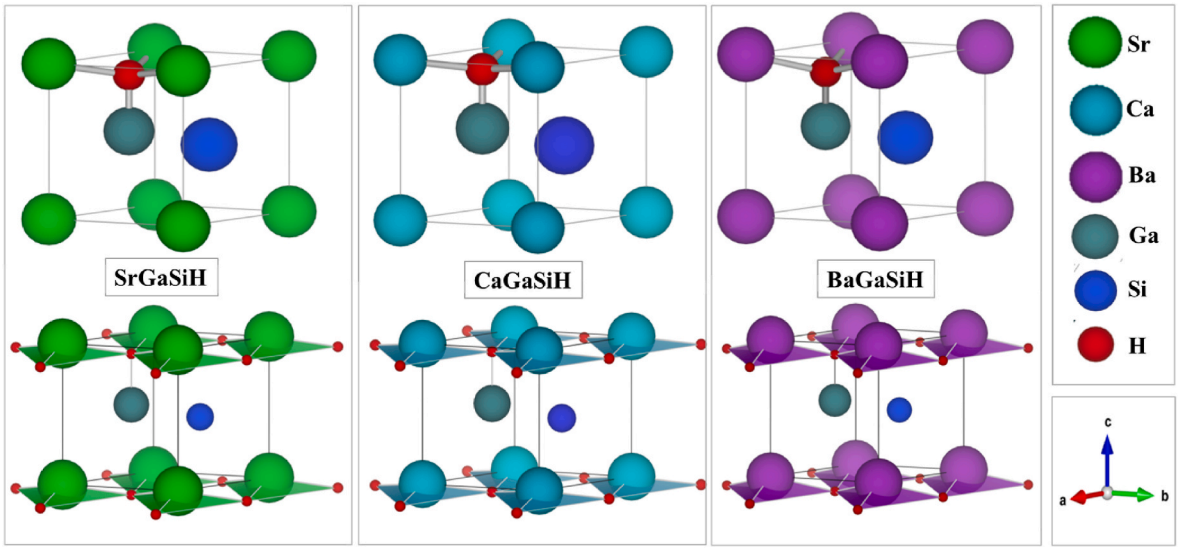

Fig. 1. Crystal structures of Hexagonal XGaSiH, with X encompassing Strontium (Sr), Calcium (Ca), and Barium (Ba).

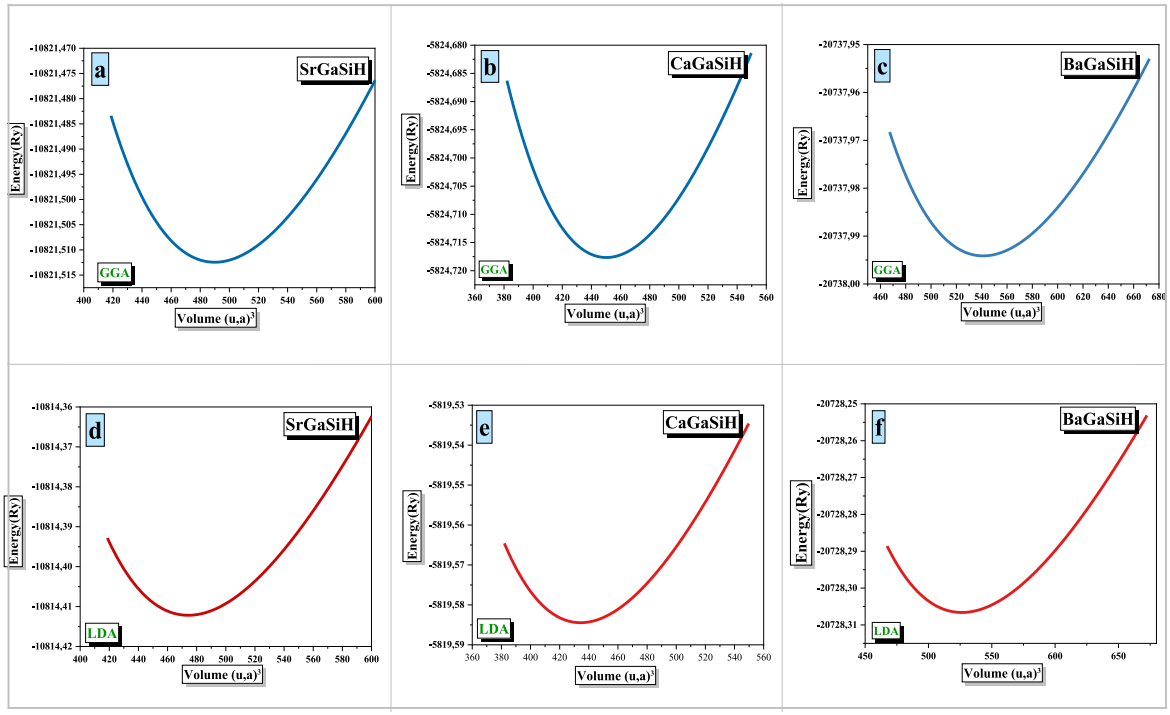

Fig. 2. Changes in total energy relative to unit cell volume, utilizing GGA(a,b,c) and LDA(d,e,f) methods for XGaSiH compounds (X = Sr, Ca, and Ba).

Table 1
Atomic positions of XGaSiH (X = Sr, Ca, and Ba) determined using LDA and GGA approximations.

Compounds	Atomic Positions (z)			Other Calculation
	(x y z)	GGA	LDA	
SrGaSiH	**Sr (0 0 z)**	**0**	**0**	**0** [29]
***P*3*m*1**	**Ga (2/3 1/3 z)**	**0.551**	**0.551**	**0.542** [29]/**0.549** [60]
	Si (1/3 2/3 z)	**0.447**	**0.447**	**0.439** [29]/**0.444** [60]
	H (2/3 1/3 z)	**0.910**	**0.909**	**0.900** [29]/**0.903** [60]
CaGaSiH	**Ca (0 0 z)**	**0**	**0**	**0** [60]
***P*3*m*1**	**Ga (2/3 1/3 z)**	**0.556**	**0.556**	**0.556** [60]
	Si (1/3 2/3 z)	**0.433**	**0.433**	**0.433** [60]
	H (2/3 1/3 z)	**0.925**	**0.925**	**0.925** [60]
BaGaSiH	**Ba (0 0 z)**	**0**	**0**	**0** [29]
***P*3*m*1**	**Ga (2/3 1/3 z)**	**0.556**	**0.556**	**0.537** [29]/**0.542** [60]
	Si (1/3 2/3 z)	**0.433**	**0.433**	**0.448** [29]/**0.455** [60]
	H (2/3 1/3 z)	**0.925**	**0.925**	**0.874** [29]/**0.875** [60]

material's stability and potential applications, particularly in the context of hydrogen storage and other energy-related technologies.

The examination of the compositions of CaGaSiH, SrGaSiH, and BaGaSiH reveals intriguing attributes related to their structural and mechanical properties. As one transitions from calcium to barium, there is a noticeable increase in cell size, reflecting the differences in ionic radii and properties between Ca^{2+}, Sr^{2+}, and Ba^{2+}. This variation impacts the overall lattice dimensions and contributes to the observed differences in material properties.

The materials under investigation demonstrate a lower bulk modulus in their initial phase compared to typical metallic hydrides, suggesting that they are more amenable to shaping and exhibit greater susceptibility to compression. Notably, BaGaSiH shows a markedly lower bulk modulus compared to SrGaSiH and CaGaSiH, leading to a greater equilibrium volume and establishing BaGaSiH as the most compressible among the studied compounds.

The relatively soft properties of the XGaSiH compounds (where X represents Sr, Ca, and Ba) can be attributed to the comparatively weak bonding interactions between the X–Ga, X–Si, and Ga–Si elements. Despite the flexibility of the Ga–H bonds within the matrix, these bonds exhibit considerable strength. Table 3 presents the measured interatomic distances in SrGaSiH, CaGaSiH, and BaGaSiH. Notably, the distances between Ga and H atoms remain consistently around 1.72 Å across the different compounds, irrespective of the specific alkaline-earth metal.

The X-Ga-Si-H bond lengths in XGaSiH compounds are closely clustered, with measurements of 2.43 Å, 2.36 Å, and 2.52 Å for SrGaSiH, CaGaSiH, and BaGaSiH, respectively. These results are in line with previous studies [26–32]. Additionally, research by Evans et al. [33] indicates that Ga–H bond lengths in similar hydrides, such as SrGaGeH, BaGaSiH, BaGaGeH, and BaGaSnH, theoretically vary from 1.764 Å to 1.772 Å, and empirically range from 1.711 Å to 1.725 Å. The distances between the Ae (Ca, Sr, Ba) atoms in these compounds span from 2.482 Å to 2.713 Å, as observed in experiments. These variations are primarily due to differences in the surrounding atomic environment.

XGaSiH compounds exhibit a stable hexagonal crystalline structure with precisely arranged Ga and Si layers. This stable structure provides a robust framework that can enhance the compounds' ability to absorb and release hydrogen effectively. The stability of the crystalline structure under varying pressure and temperature conditions further improves the ability of these compounds to retain and release hydrogen as needed.

3.2. Electronic structure

Fig. 3 presents the energy band structures of XGaSiH compounds (X = Sr, Ca, Ba) along various high-symmetry paths within the Brillouin zone. The calculations of these band structures utilized several computational methods, including Generalized Gradient Approximation (GGA), Local Density Approximation (LDA), and the modified Becke-Johnson approximations (mBJ-GGA and mBJ-LDA). These modified methods build upon traditional Density Functional Theory (DFT) to enhance the precision of electronic property predictions in semiconductors and insulators.

In the hexagonal phases of XGaSiH, the valence band exhibits a peak

Table 2
Calculated lattice constants (a, c and c/a) in Å, bulk modulus (B) in GPa and pressure derivative (B′) at equilibrium volume using GGA and LDA compared to experimental findings of XGaSiH (X = Sr, Ca, and Ba) compound.

Compounds (structure type; space group)	Lattice Parameters			Experiment Value	Relative error		
		GGA	LDA			GGA	LDA
SrGaSiH ***P*3*m*1**	**a**	**4.146**	**4.100**	**4.188** [60]/**4.194** [26]	$\nabla a/a\|_{Exp}$	**−0.009/-0.011**	**−0.021/-0.022**
	c	**4.869**	**4.802**	**5.002** [60]/**4.948** [26]	$\nabla c/c\|_{Exp}$	**−0.027/-0.016**	**−0.041/-0.030**
	c/a	**1.174**	**1.171**	**1.190** [60]	$\nabla c/c\|_{Exp}$	**−0.013**	**−0.016**
	B(Gpa)	**61.859**	**67.994**	**58.000** [26]			
	B'	**4.315**	**4.449**				
	V(Å^3)	**72.625**	**70.317**	**75.989** [60]/**75.388** [26]	$\nabla V/V\|_{Exp}$	**−0.046/-0.038**	**−0.080/-0.072**
CaGaSiH ***P*3*m*1**	**a**	**4.045**	**3.997**	**4.091** [60]	$\nabla a/a\|_{Exp}$	**−0.011**	**−0.023**
	c	**4.669**	**4.593**	**4.762** [60]	$\nabla c/c\|_{Exp}$	**−0.019**	**−0.036**
	c/a	**1.154**	**1.149**	**1.160** [60]			
	B(Gpa)	**67.819**	**72.709**	**59.000** [26]			
	B'	**3.941**	**4.198**				
	V(Å^3)	**66.732**	**64.399**	**69.035** [60]	$\nabla V/V\|_{Exp}$	**−0.034**	**−0.071**
BaGaSiH ***P*3*m*1**	**a**	**4.228**	**4.190**	**4.301** [60]/**4.321** [26]	$\nabla a/a\|_{Exp}$	**−0.017/-0.022**	**−0.026/-0.031**
	c	**5.115**	**5.133**	**5.270** [60]/**5.190** [26]	$\nabla c/c\|_{Exp}$	**−0.030/-0.014**	**−0.026/-0.011**
	c/a	**1.209**	**1.211**	**1.220** [60]			
	B(Gpa)	**56.935**	**62.032**	**48.000** [26]			
	B'	**4.472**	**4.612**				
	V(Å^3)	**80.231**	**78.053**	**84.451** [60]/**83.956** [26]	$\nabla V/aV\|_{Exp}$	**−0.052/-0.046**	**−0.081/-0.075**

Table 3
The lengths of atomic bonds (Å) and angles (°) in in XGaSiH (X = Sr, Ca, Ba) compounds.

	SrGaSiH			CaGaSiH			BaGaSiH		
	GGA	LDA	Experimental	GGA	LDA	Experimental	GGA	LDA	Experimental
Ga–Si (×3)	**2.447**	**2.421**	**2.475** [26]	**2.405**	**2.461**		**2.481**	**2.461**	**2.512** [30]
X–H(×3)	**2.433**	**2.405**	**2.472** [26]	**2.361**	**2.376**	**2.390** [31]	**2.522**	**2.500**	**2.532** [30]
X–Si(×3)	**3.600**	**3.554**		**3.527**	**3.477**	**3.105** [31]	**3.703**	**3.692**	**3.485** [61]
X–Ga(×3)	**3.239**	**3.192**	**3.279** [26]	**3.120**	**3.077**		**3.382**	**3.363**	**3.363** [62]
Ga–H(×1)	**1.745**	**1.712**	**1.771** [26]	**1.719**	**1.719**	**1.706** [31]	**1.706**	**1.703**	**1.726** [22]
Ga-Si-Ga(×3)	**115.833**	**115.696**		**114.476**	**114.476**		**116.870**	**116.694**	
Si-Ga-Si(×3)	**115.833**	**115.696**		**114.476**	**114.476**		**116.870**	**116.694**	
Si-Ga-H(×3)	**101.943**	**102.145**		**103.827**	**103.827**		**100.308**	**100.600**	

at the M point of the Brillouin zone, while the conduction band reaches its minimum along the σ-K direction. This observation indicates an indirect band gap between the M point and the σ-K direction. Despite some variations in the precise values, the band structures of these compounds display qualitatively similar characteristics, highlighting consistent electronic behavior across the series.

The bandgap energies of XGaSiH compounds were determined using various computational approaches. For SrGaSiH, the Generalized Gradient Approximation (GGA) method yielded a bandgap of 0.380 eV, while the Local Density Approximation (LDA) method provided a bandgap of 0.333 eV. Enhanced methods, such as modified Becke-Johnson GGA (mBJ-GGA) and modified Becke-Johnson LDA (mBJ-LDA), produced higher bandgaps of 0.942 eV and 0.933 eV, respectively. Previous Density Functional Theory (DFT) calculations reported bandgaps of 0.47 eV and 0.6 eV. For CaGaSiH, the GGA method indicated a bandgap of 0.170 eV, while the LDA method yielded a lower bandgap of 0.100 eV. The mBJ-GGA and mBJ-LDA methods reported bandgaps of 0.702 eV and 0.635 eV, respectively, whereas DFT calculations showed bandgaps of 0.28 eV and 0.3 eV. For BaGaSiH, the bandgap values were 0.478 eV for GGA, 0.542 eV for LDA, 0.980 eV for mBJ-GGA, and 0.974 eV for mBJ-LDA. DFT methods reported bandgaps of 0.53 eV and 0.6 eV.

These variations in bandgap values highlight the influence of the computational method used, with DFT methods typically underestimating bandgaps due to discontinuities in the exchange-correlation potential. Analysis of the band structures indicates that the conduction and valence bands in XGaSiH compounds are separated by bandgap energies ranging from 0.1 eV to 0.9 eV. This suggests that these compounds exhibit significant conductivity, attributed to their very small bandgaps.

Table 4 summarizes the energy gap values obtained using various approximations. These bandgap values align with previous research conducted by P. Vajeeston et al. [34], who calculated bandgaps using the DFT method with the GGA-PBE functional. It is well recognized that the GGA-PBE functional systematically underestimates bandgap values due to inherent discontinuities in the exchange-correlation potential. For example, Vajeeston et al. reported bandgaps for SrGaSiH, CaGaSiH, and BaGaSiH as 0.6 eV, 0.3 eV, and 0.6 eV, respectively. In comparison, John A. et al. [13]reported bandgap values of 0.47 eV, 0.28 eV, and 0.53 eV for these compounds using the Quantum Espresso package with the GGA approximation. Additionally, the bandgap energies observed in this study are in reasonable agreement with those reported for XAlSiH hydride compounds (X = Sr, Ca, Ba) [35].

Fig. 4 presents the density of states (DOS) curves for the ground-state

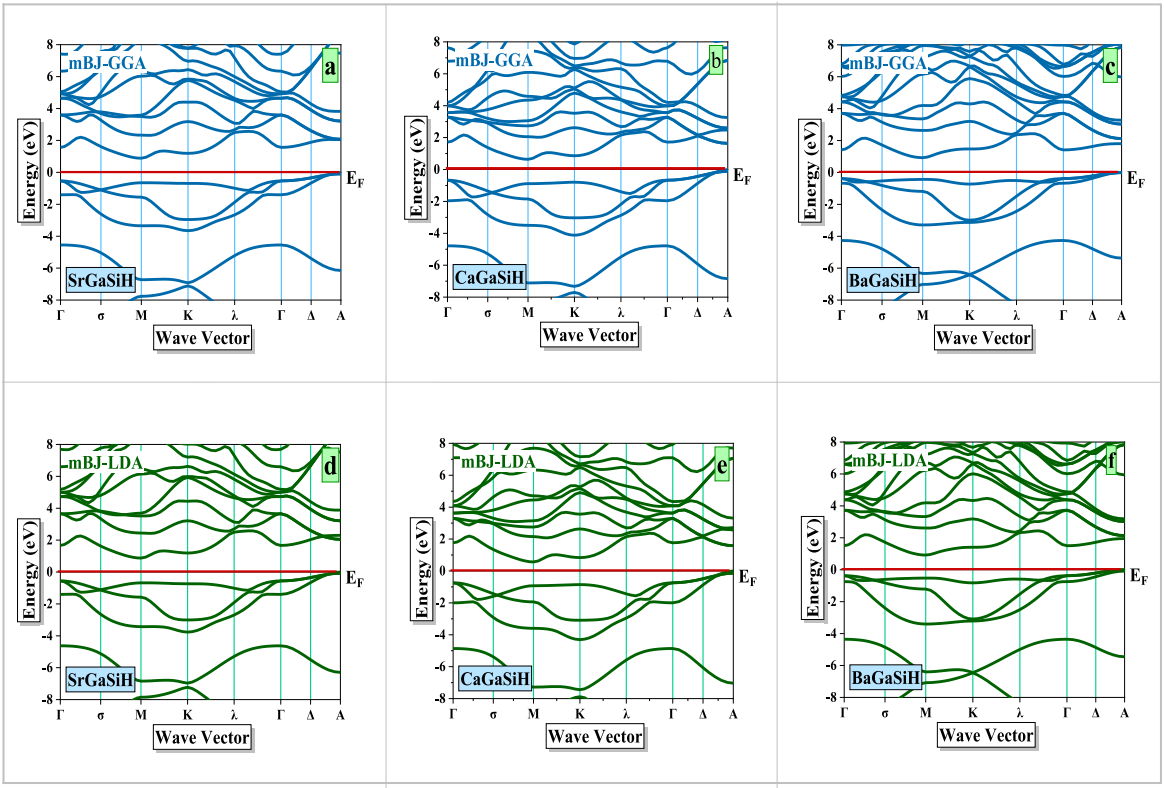

Fig. 3. The band structure along the symmetry paths in the Brillouin Zone for XGaSiH compounds (with X being Sr, Ca, and Ba) in a primitive hexagonal lattice (*P*3*m*1). using mBJ-GGA(a,b,c), and mBJ-LDA(d,e,f) methods. The graph is scaled for 0 eV at the Fermi level (E_F).

Table 4
The energy gap E_g calculated in different approximations.

Compounds	Bandgap (eV)				
	GGA	LDA	MBJ-GGA	MBJ-LDA	DFT
SrGaSiH (*P*3*m*1)	**0.380**	**0.333**	**0.942**	**0.933**	**0.47** [13]/**0.6** [34]
CaGaSiH (*P*3*m*1)	**0.170**	**0,100**	**0.702**	**0.635**	**0,28** [13]/**0,3** [34]
BaGaSiH (*P*3*m*1)	**0.478**	**0.542**	**0.980**	**0.974**	**0.5 3** [13]/**0.6** [34]

phases of XGaSiH compounds (where X = Sr, Ca, and Ba) at their equilibrium volumes. The DOS curves were generated using GGA, LDA, mBJ-GGA, and mBJ-LDA approximations. For SrGaSiH, the total DOS curve reveals a valence band extending from −10 eV to the Fermi level (0 eV), with two distinct regions. The first region, from −10.25 eV to −4.54 eV, is predominantly influenced by the *s*-states of Ga, Si, and H, which shape the electronic configuration. The second region, extending from −4.34 eV to the Fermi level, is dominated by the *p*-states of Ga and Si, alongside the s-states of H. The DOS distribution for the XGaSiH-LDA approximation mirrors this pattern with minor variations in state contributions, while the XGaSiH-mBJ-GGA and SrGaSiH-mBJ-LDA approximations exhibit a broadened valence band and improved accuracy in the electronic structure calculations.

For CaGaSiH, the total DOS curve displays a valence band spanning from −11 eV to 0 eV, delineated into two regions. The first region, from −11 eV to −8 eV, is prominently influenced by the *s*-states of Si. The second region, from −7.36 eV to E_F, is characterized by the *s*-states of Si and H, with significant contributions from Si *p*-states. The BaGaSiH material has a total density of states (DOS) curve that encompasses a valence band spanning from −9 eV to 0 eV. This valence band can be further categorized into two separate sections. The initial range, spanning from −9 eV to −4.25 eV, is notably influenced by the s-orbitals of Ga, Si, and H. The second zone, ranging from −3.54 eV to the Fermi energy (E_F), is primarily characterized by the *s*-states of hydrogen (H) and the *p*-states of gallium (Ga), with significant contributions from silicon (Si) *p*-states. It is worth mentioning that the interaction between hydrogen states and the *s* and *p* orbitals of silicon, as well as the *s* and *p* orbitals of gallium, can be observed. The characteristics of the valence bands around the Fermi level are mostly influenced by the silicon p-orbitals and hydrogen states.

A notable trend observed in SrGaSiH, CaGaSiH, and BaGaSiH is the clear reduction in the energy difference between the lowest and highest valence bands. This reduction could significantly influence their electrical properties. Each of these hydrides exhibits a relatively narrow energy gap between the valence and conduction bands, indicating semiconductor-like behavior, which is consistent with the characteristics observed in the previously studied SrAlSiH system.

Although the DOS trends across SrGaSiH, CaGaSiH, and BaGaSiH show general similarities, there are notable variations in state contributions among these compounds. The mBJ approximations enhance the precision of these calculations by broadening the energy ranges and providing a more accurate depiction of the electronic structure. This improvement allows for a deeper and more comprehensive understanding of the electrical properties of these hydrides.

XGaSiH compounds possess small energy gaps ranging from 0.1 to 0.9 electron volts, indicating the potential for high conductivity. This suggests that these compounds can quickly respond to changes in electrical charges during the absorption or release of hydrogen, facilitating the storage and release process. The narrow gaps increase the likelihood of forming effective bonds between hydrogen and the compounds, thereby enhancing storage performance.

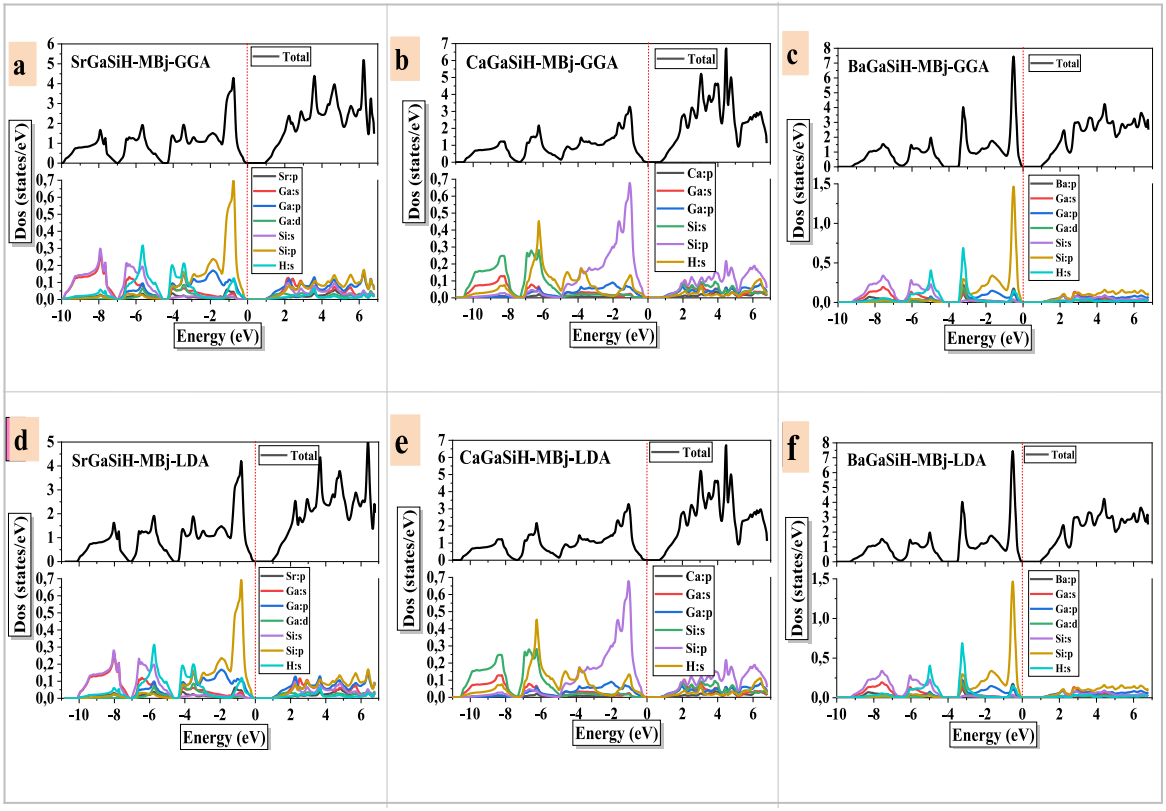

Fig. 4. The total and partial Density of States (DOS) for XGaSiH systems (X = Sr, Ca, Ba), derived from mBJ-GGA (a,b,c), and mBJ-LDA (d,e,f)computational approximations.

3.3. Thermodynamic properties

Fig. 5 illustrates the predicted equilibrium volumes of the compounds SrGaSiH, CaGaSiH, and BaGaSiH under varying pressure levels and temperatures. As the temperature increases, there is a notable expansion in the overall volume of these crystals. This behavior is consistent with the observed changes in volume for related compounds such as SrAlSiH, CaAlSiH, and BaAlSiH. Notably, the equilibrium volume of these materials increases with rising temperature, particularly at a pressure of 0 GPa. This trend highlights the inherent flexibility of these compounds, as they exhibit significant volumetric expansion in response to thermal changes.

Understanding the thermodynamic properties of materials is essential for assessing their stability and suitability for various applications, particularly those involving fluctuating environmental conditions. Thermodynamic analysis provides insights into how materials respond to changes in temperature and pressure, which is crucial for predicting their performance and reliability in real-world scenarios.

To thoroughly evaluate these properties, ab-initio calculations using the quasiharmonic approximation are employed. This advanced computational approach allows for an accurate assessment of phonon effects—quantum mechanical descriptions of lattice vibrations—across a broad temperature range from 0 to 1000 K. By incorporating these vibrational effects, the quasiharmonic approximation accounts for temperature-induced changes in the material's properties, such as thermal expansion and heat capacity.

Moreover, the quasiharmonic approximation is also applied under varying pressure conditions, up to 50 GPa, which enables the

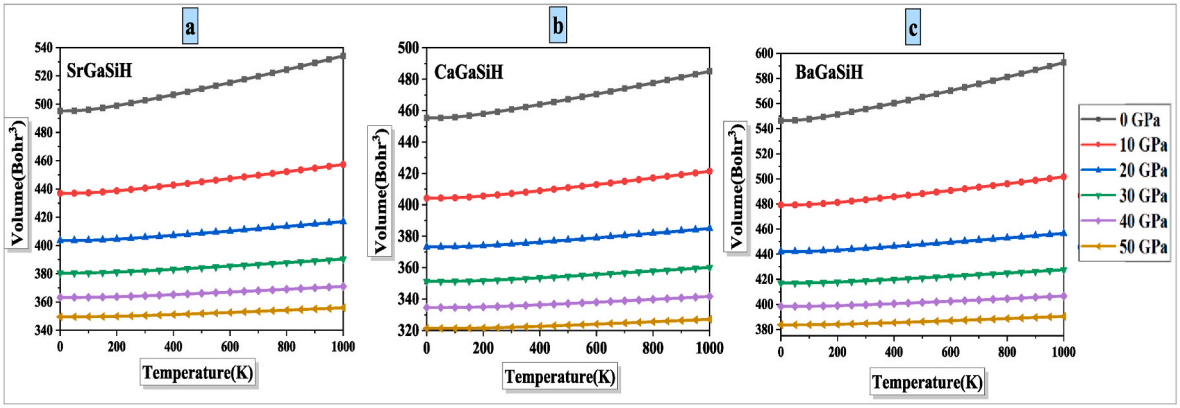

Fig. 5. Variation of the volume cell as a function of the temperature for SrGaSiH, CaGaSiH and BaGaSiH, respectively. **(a), (b)** and **(c)**.at different pressures, using GGA.

exploration of how materials behave under extreme compression. This pressure range is particularly relevant for understanding the material's stability and phase transitions under high-pressure environments, which are often encountered in practical applications or experimental settings.

By integrating these factors, the quasiharmonic approximation provides a comprehensive view of the material's thermal behavior, including how its lattice structure adapts to thermal and pressure-induced stresses. This approach ensures a detailed understanding of the material's stability, enabling the prediction of its performance and durability in various conditions.

Such detailed thermodynamic analysis is invaluable for designing materials for specific applications, such as high-temperature or high-pressure environments, and for ensuring their reliability and efficiency in practical use. The insights gained from these calculations support the development of advanced materials with tailored properties, enhancing their functionality and expanding their potential applications in fields such as energy storage, catalysis, and materials science.

The bulk modulus, which measures a material's resistance to uniform compression, exhibits stability within the temperature range of 0–200 K, but then decreases linearly with increasing temperature. This trend indicates that as temperature rises, the material becomes more compressible, as illustrated in Fig. 6. For instance, at 0 K, the bulk modulus values obtained are 66.31 GPa for CaGaSiH, which aligns closely with the GGA results of 67.81 GPa. Similarly, SrGaSiH has a calculated bulk modulus of 60.36 GPa, nearly matching the value of 61.85 GPa, and BaGaSiH shows a bulk modulus of 55.64 GPa, close to 56.93 GPa. These results suggest that CaGaSiH is the most compressible of the three, with the bulk modulus consistently decreasing as temperature increases, reflecting a direct relationship between temperature and compressibility.

The Debye temperature (θ_D) is crucial for understanding how a crystal behaves at different temperature regimes. It represents a threshold above which vibrational modes reach thermal equilibrium. Fig. 7 shows the temperature-dependent Debye temperature for XGaSiH compounds (X = Sr, Ca, Ba) under varying pressures. The Debye temperature, which reflects the strength of interatomic bonds and the material's hardness, is 361.15 K for SrGaSiH, 432.62 K for CaGaSiH, and 313.54 K for BaGaSiH at 0 K. Generally, higher Debye temperatures indicate greater hardness. However, the hardness of XGaSiH crystals decreases under low pressure, though this effect can be mitigated by applying pressure, highlighting the flexibility and response of these compounds to external conditions.

Figs. 8 and 9 show the specific heat capacities at constant pressure (C_p) and constant volume (C_v), respectively. Unfortunately, there are no previous results available for direct comparison. The heat capacity of a material can be assessed by examining its vibrational properties through thermodynamic measurements. These measurements are essential for understanding how the material's thermal characteristics vary with pressure and temperature. At low temperatures, C_v correlates directly with T^3, consistent with classical mechanics' equipartition theory, which posits that the kinetic energy of each atom is proportional to its degrees of freedom. This correlation indicates that as temperature increases, the available energy for atomic motion increases, resulting in a cubic increase in C_v. Fig. 8 clearly demonstrates that temperature has a more pronounced effect on C_p compared to pressure, with C_p heat capacity curves following the classical Dulong and Petit law at higher temperatures. Quantum oscillators, or phonons, exhibit activation of low-energy acoustic modes at low temperatures. At standard temperature and pressure, the specific heat capacities (C_v and C_p) for BaGaSiH, CaGaSiH, and SrGaSiH are approximately 98.55 (107.65), 96.82 (102.86), and 97.67 (105.87) J $mol^{-1}K^{-1}$, respectively. Temperatures above 500 K, where C_p exceeds C_v, indicate thermodynamic stability.

Entropy (S), representing disorder or randomness in a material, increases with temperature and pressure. At room temperature and standard conditions, the entropy values for SrGaSiH, CaGaSiH, and BaGaSiH are 173.11, 153.90, and 187.86, respectively. As illustrated in Fig. 10, entropy increases with temperature, reflecting the material's tendency towards greater disorder with rising thermal energy.

The thermal expansion coefficient (α), which measures a material's volume change in response to temperature changes, becomes challenging to measure accurately at high temperatures due to significant volume adjustments. Accurate measurements at these conditions require precise and analytical techniques, given the unique challenges involved. Real materials exhibit anharmonic interactions where phonons respond to temperature changes with increased activation, leading to lattice expansion. This anharmonicity causes the thermal expansion coefficient to vary with temperature, illustrating the complex interplay between anharmonic interactions and thermal expansion. Fig. 11 illustrates how temperature and pressure influence the coefficients of thermal expansion for XGaSiH compounds (X = Sr, Ca, Ba). The data show a direct correlation between temperature and expansion coefficients from 400 to 1000 K, with a notable increase up to 400 K. Additionally, the coefficient decreases with increasing pressure, suggesting that temperature effects become less significant at high pressures, highlighting the role of anharmonic effects in these materials' thermal expansion. At 0 GPa and room temperature, the thermal expansion coefficients for SrGaSiH, CaGaSiH, and BaGaSiH are approximately 9.45×10^{-5} K^{-1}, 7.85×10^{-5} K^{-1}, and 10.14×10^{-5} K^{-1}, respectively, showing notable similarities among these materials.

As for the impact of thermodynamic properties on the hydrogen storage mechanism, the results of the thermal expansion coefficient indicate that XGaSiH compounds expand significantly with increasing temperature, particularly at low pressure. This expansion facilitates more effective hydrogen storage under high thermal conditions, where the crystal structure can accommodate hydrogen atoms without losing structural stability. Additionally, the results showed that the heat

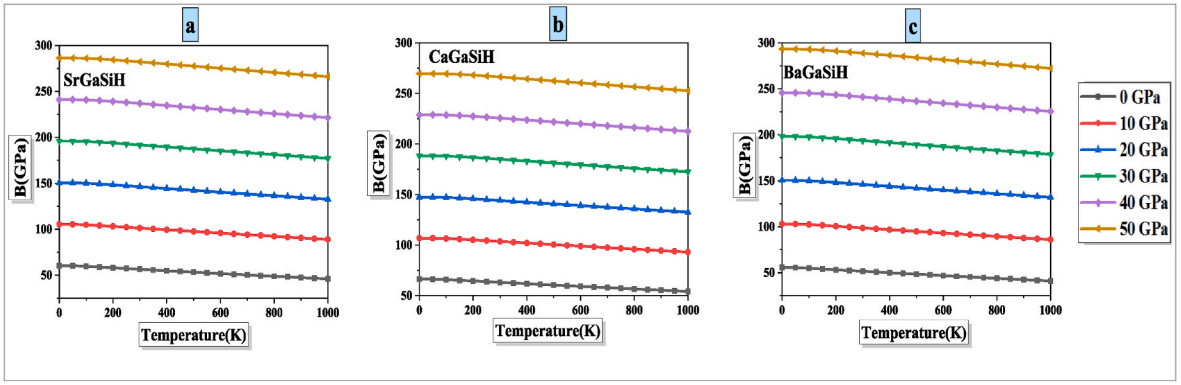

Fig. 6. Variation of the bulk modulus as a function of the temperature for SrGaSiH, CaGaSiH and BaGaSiH, respectively. **(a), (b)** and **(c)**. at different pressures, using GGA.

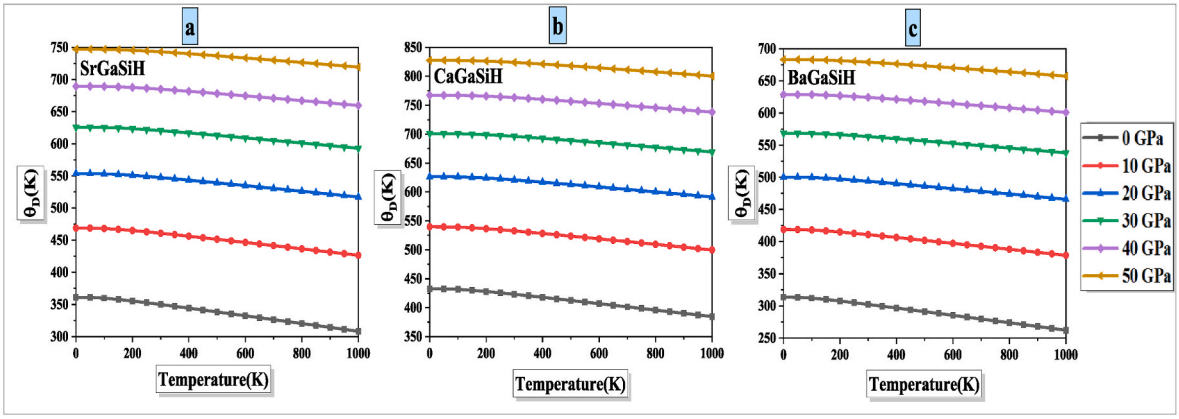

Fig. 7. Variation of the Debye temperature θ_D as a function of the temperature for SrGaSiH, CaGaSiH and BaGaSiH, respectively. **(a), (b)** and **(c)**. at different pressures, using GGA.

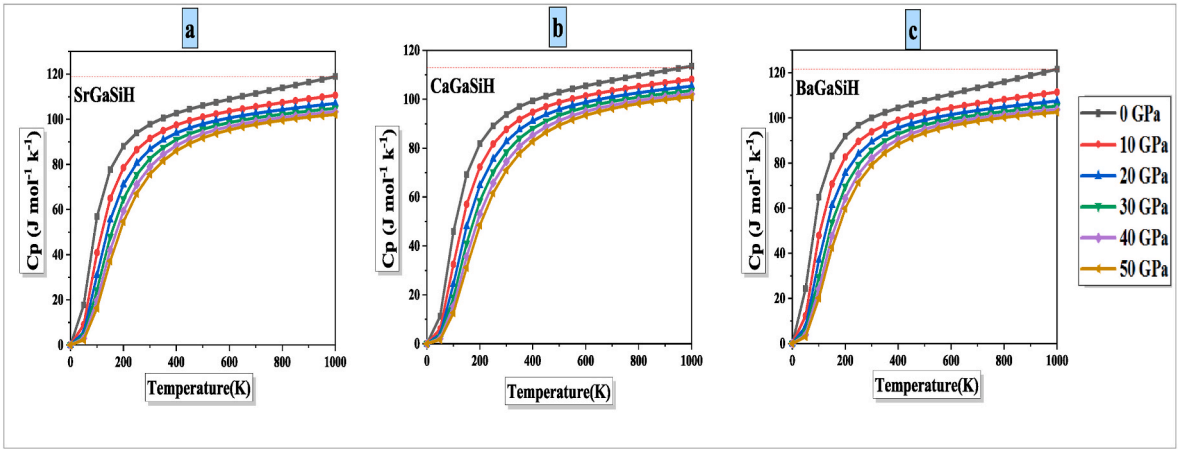

Fig. 8. Variation of the heat capacity C_p versus temperature for SrGaSiH, CaGaSiH and BaGaSiH, respectively. **(a), (b)** and **(c)**.at different pressures, using GGA.

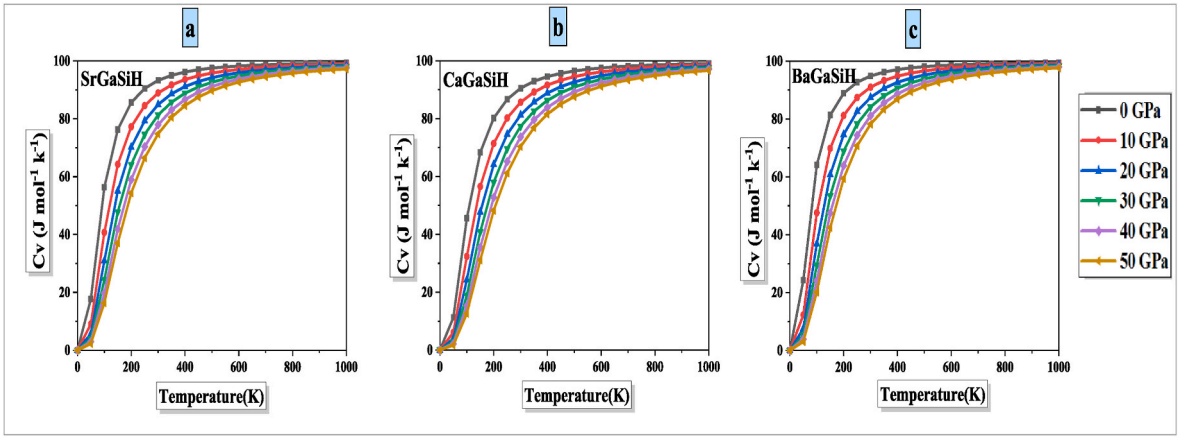

Fig. 9. Variation of the heat capacity C_v versus temperature for SrGaSiH, CaGaSiH and BaGaSiH, respectively. **(a), (b)** and **(c)**. at different pressures, using GGA.

capacity of the compounds increases with temperature, indicating their ability to absorb large amounts of heat during hydrogen absorption. This thermal absorption is crucial for facilitating the processes of hydrogen absorption and release at various temperatures, making these compounds suitable for hydrogen storage in diverse operational conditions. Furthermore, the Debye temperature is an important indicator of the stability of atomic bonds in the compounds at different temperatures. The high Debye temperature values in XGaSiH compounds indicate strong atomic bonds and their ability to withstand the thermal vibrations caused by hydrogen interaction with the material, ensuring that the compounds can store hydrogen safely and stably even at elevated temperatures. The Gibbs free energy variation results over a wide range of temperatures and pressures suggest that XGaSiH compounds maintain their thermodynamic stability, ensuring that hydrogen remains trapped within the crystal structure until significant changes in thermal and pressure conditions occur, allowing controlled hydrogen release when

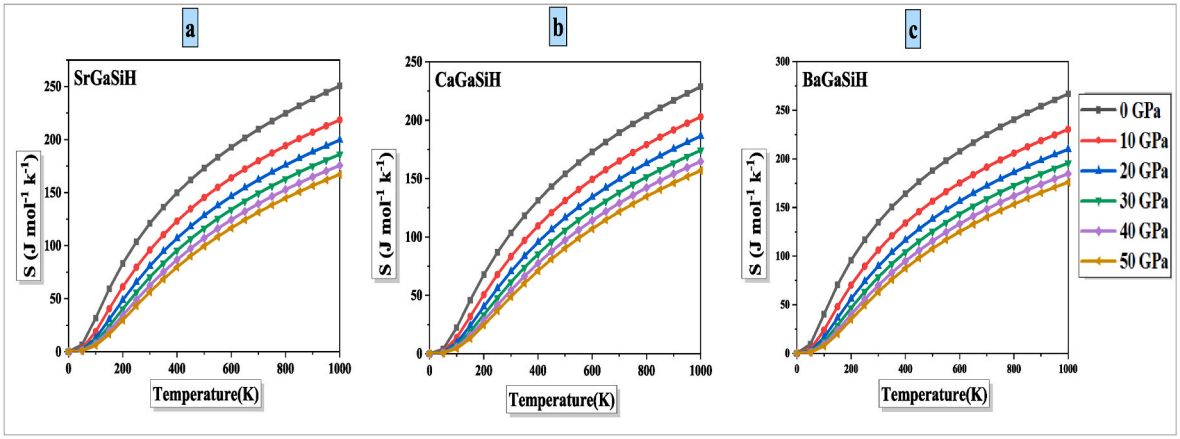

Fig. 10. Variation of the entropy S as a function of the temperature for SrGaSiH, CaGaSiH and BaGaSiH, respectively. **(a), (b)** and **(c)**. at different pressures, using GGA.

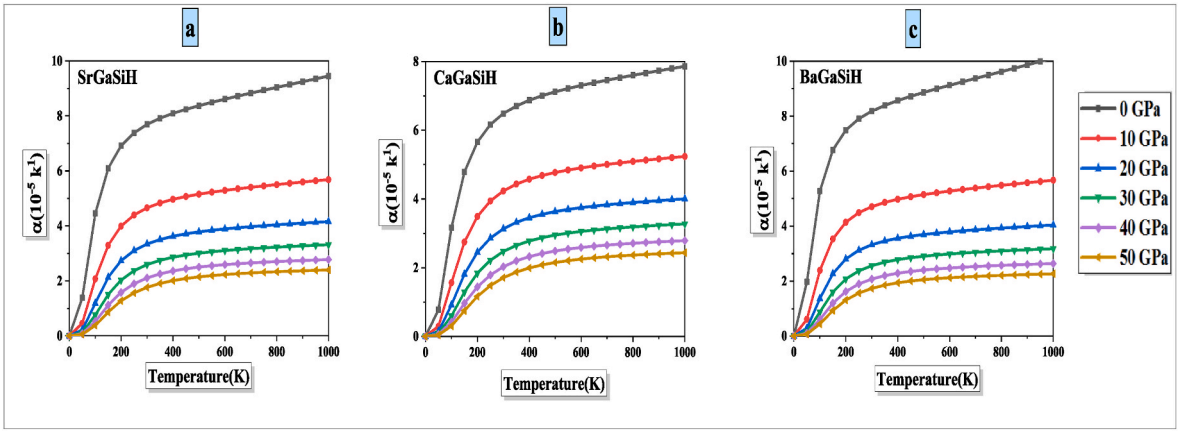

Fig. 11. Variation of thermal expansion α as a function for SrGaSiH, CaGaSiH and BaGaSiH, respectively. **(a), (b)** and **(c)**. at different pressures, using GGA.

needed. Finally, the values of Helmholtz free energy and the Grüneisen parameter provide additional indicators of the compounds' stability under the influence of heat and pressure, where positive values indicate the compounds' ability to maintain their structural integrity during hydrogen storage in various operational environments.

3.4. Properties of hydrogen storage

The gravimetric hydrogen storage capacity (Cw %) measures how much hydrogen a material can store relative to its mass. This metric is important for assessing a material's ability to absorb hydrogen and is usually reported as weight percent (wt %). It is crucial for evaluating the material's suitability for hydrogen storage systems in applications like fuel cells or hydrogen vehicles. A recent study examined the hydrogen storage capacities of various hydrides, including XGaSiH (where X is Sr, Ca, and Ba), using equation (15) from Ref. [36] to calculate these capacities from experimental data.

$$CW\% = \left(\frac{\left(\frac{H}{M}\right) M_H}{M_{Host} + \left(\frac{H}{M}\right) M_H} \times 100 \right) \% \quad (15)$$

Based on the results derived from Equation (15), we can accurately compute the weight percentage of hydrogen stored within each material. This computation reveals the gravimetric hydrogen storage capacities for SrGaSiH, CaGaSiH, and BaGaSiH to be 0.34 wt %, 0.47 wt %, and 0.40 wt %, respectively. These values represent the percentage of the material's weight that is attributable to stored hydrogen, providing a crucial metric for evaluating the effectiveness of these compounds in hydrogen storage applications.

The term 'H/M' is used to denote the hydrogen-to-material atom ratio. This ratio measures the proportion of hydrogen atoms relative to the total number of atoms in the material, offering insight into the material's capacity to host hydrogen relative to its atomic composition. In the context of hydrogen storage, 'H' represents the mass of hydrogen that is absorbed or stored within the material, while 'M' refers to the total mass, which is the sum of the masses of both the hydrogen and the host material.

To clarify further, M_H denotes the molar mass of hydrogen, which is used to convert between the mass of hydrogen and the number of hydrogen atoms.

M_{Host}, on the other hand, refers to the molar mass of the host material, excluding hydrogen. By using these parameters, we can accurately determine how much hydrogen is stored per unit weight of the material, providing valuable information about the efficiency of the material as a hydrogen storage medium. This detailed understanding of gravimetric hydrogen storage capacities and the hydrogen-to-material ratio is essential for assessing the practicality and performance of these materials in real-world applications, such as fuel cells and other hydrogen storage technologies. Evaluating these parameters helps in optimizing material selection and enhancing the design of systems that rely on efficient hydrogen storage solutions.

Furthermore, the desorption temperature, T_D, is a critical parameter in evaluating materials for hydrogen storage. This temperature

represents the threshold at which hydrogen is released from the material when subjected to heating. It is a key factor in assessing the practicality of the material for hydrogen storage applications, as it affects the efficiency and safety of hydrogen release. The desorption temperature can be calculated using the Gibbs-Helmholtz equation, which relates the temperature to the enthalpy and entropy changes of the desorption process. This equation is detailed in Equation (16) from Ref. [37], and provides a quantitative measure of how temperature influences the release of hydrogen from the material.

$$\Delta S = \frac{\Delta H - \Delta G}{T} \tag{16}$$

ΔG represents the standard Gibbs free energy change for the hydrogen dehydrogenation reaction, ΔH denotes the enthalpy change (specifically, the enthalpy of formation), and ΔS signifies the entropy change associated with the reaction. At equilibrium, the change in Gibbs free energy (ΔG) is zero, which indicates that there is no net change in the system's free energy, and the reaction has reached its equilibrium state.

To calculate the desorption temperature (T_D), the formula used is given by Ref. [38]:

$$T_D = \frac{\Delta H}{\Delta S} \tag{17}$$

This formula derives from the Gibbs-Helmholtz equation, which connects the desorption temperature to the enthalpy and entropy changes of the dehydrogenation reaction. By applying this formula, one can determine the temperature at which hydrogen is released from the material, thus providing a key parameter for evaluating the material's suitability for hydrogen storage applications.

Here, ΔH in the context of hydrogen dehydrogenation reactions typically represents a positive value, as these reactions are often endothermic, meaning they require heat input to proceed. This ΔH should not be confused with the enthalpy of formation, which is generally negative as it refers to the energy released when the material is formed from its elements. ΔS represents the entropy change associated with the dehydrogenation reaction. The formula, derived from the Gibbs-Helmholtz equation, relates the desorption temperature to the enthalpy and entropy changes of the reaction, providing a crucial parameter for evaluating the material's performance in hydrogen storage applications.

Specific values for T_D and ΔS were calculated for the compounds CaGaSiH (ΔS = 143.18 J/mol.K, T_D = 587.39 K), BaGaSiH (ΔS = 174.82 J/mol.K,T_D = 346.50 K), and SrGaSiH (ΔS = 161.02 J/mol.K, T_D = 457.62 K). These values are critical for assessing the efficiency and suitability of these materials for hydrogen storage applications. The desorption temperature (T_D) indicates the temperature at which hydrogen is released from the material, which is a key parameter for practical applications. Higher T_D values, such as that for CaGaSiH (587.39 K), suggest that the material requires higher temperatures to release hydrogen, which may affect the efficiency of hydrogen storage and release processes. In contrast, materials with lower T_D values, like BaGaSiH (346.50 K), release hydrogen at lower temperatures, potentially making them more suitable for applications requiring easier and more energy-efficient hydrogen release.

The entropy change (ΔS) provides insight into the disorder or randomness associated with the hydrogen release process. Larger ΔS values indicate a greater increase in entropy during hydrogen release, which often corresponds to more favorable thermodynamic conditions for the dehydrogenation reaction. For instance, BaGaSiH with the highest ΔS (174.82 J/mol·K) may demonstrate a more significant increase in disorder, potentially enhancing its efficiency as a hydrogen storage material under certain conditions.

Overall, understanding these specific values allows researchers to better evaluate the potential of these materials in hydrogen storage applications, particularly in the context of sustainable and clean energy technologies. Materials with suitable desorption temperatures and entropy changes are essential for optimizing hydrogen storage systems to meet the energy demands of future clean energy solutions.

3.5. Elastic properties

Elastic constants are fundamental for understanding the mechanical and dynamic properties of solids. They offer crucial insights into the internal forces present within crystals, as well as the rigidity and strength of crystalline materials. These constants are vital for characterizing how materials respond to external forces, determining their stability, and predicting their behavior under various conditions. Specifically, elastic constants help in understanding the material's resistance to deformation, its ability to return to its original shape after stress is applied, and its overall structural integrity.

To accurately determine these constants, potential functions of both first and second orders are often utilized. These functions describe the interactions between atoms within the crystal lattice and are essential for computational methods that predict elastic properties from first principles. Ab initio computations, which are based on fundamental physical theories without empirical parameters, are frequently employed to calculate these constants. These computations require precise methodologies to ensure accuracy and reliability [39]. Despite significant advancements in theoretical calculations, obtaining experimental data for monocrystalline elastic constants remains a challenge, often due to the complexity of measurements and the precision required.

For materials with hexagonal crystal structures, such as our compounds XGaSiH, there are six distinct elastic constants: C_{11}, C_{12}, C_{13}, C_{33}, C_{44}, and C_{66}. These constants describe different types of deformation responses in the crystal lattice. For example, C_{11} and C_{33} relate to the compressibility along the principal axes, C_{12} and C_{13} describe the coupling between different directions, and C_{44} and C_{66} are related to shear deformations. Accurate determination of these constants involves understanding how energy changes with applied stress during specific deformations. This requires a comprehensive analysis of the crystal's response to applied forces and stresses, which can be complex and computationally intensive.

The WIEN2K package is a valuable tool in this regard. It provides advanced computational capabilities to optimize the internal cell structure of crystals using force-driven optimization methodologies. This software facilitates the calculation of elastic constants by allowing precise modeling of the crystal lattice and its interactions. By leveraging WIEN2K's capabilities, researchers can achieve a more accurate and detailed understanding of the mechanical properties of hexagonal crystal structures, contributing to the development and application of advanced materials in various fields.

The stress-strain approach is a technique used to determine the elastic constants of a material by applying known stresses and measuring the resulting strains. This method involves imposing various types of stress on the material and quantifying how it deforms in response. The elastic constants Cij are essential parameters that quantify the stiffness of a material, reflecting its resistance to deformation. These constants are crucial for understanding the mechanical properties of materials and are typically calculated using the Generalized Gradient Approximation (GGA) approach in computational simulations.

In Table 5, the elastic constants for the hexagonal crystalline forms of XGaSiH (where X = Sr, Ca, and Ba) are presented. The positive values of these elastic constants confirm the mechanical stability of the compounds. Specifically, positive elastic constants indicate that the materials can withstand deformation and return to their original shape, demonstrating both stability and flexibility under stress [40].

$$\begin{cases} C_{44} > 0, C_{66} > 0, C_{11} > |C_{12}| \\ C_{11}C_{33} > C_{13}^2 \\ (C_{11} + C_{12})C_{33} - 2C_{13}^2 > 0 \end{cases} \tag{18}$$

The satisfaction of these stability criteria underscores that the

Table 5
Elastic constants of XGaSiH (X = Sr, Ca, Ba) calculated using GGA, along with the melting temperature (Tm) in Kelvin (K).

	SrGalSiH *P3m1*	CaGaSiH *P3m1*	BaGalSiH *P3m1*
C_{11}	**169.649**	**185.640**	**149.224**
C_{33}	**93.523**	**101.594**	**99.568**
C_{44}	**51.482**	**48.619**	**51.260**
C_{66}	**69.194**	**72.119**	**62.269**
C_{12}	**31.260**	**41.402**	**24.685**
C_{13}	**25.644**	**29.231**	**31.872**
T_m	**1176.457 ± 300**	**1240.953 ± 300**	**1185.850 ± 300**
A_1	**0.971**	**0.850**	**1.108**
A_2	**1**	**1**	**1**

XGaSiH compounds are both structurally stable and mechanically flexible. This makes them promising candidates for various applications that require robust and reliable material performance, including in energy storage and conversion technologies. The positive values of the elastic constants and adherence to the stability criteria affirm the potential of these materials in advanced technological applications.

Table 5 displays the elastic constants of the XGaSiH compounds (where X = Sr, Ca, and Ba) in ascending order based on their magnitude: C_{ij} (CaGaSiH) > C_{ij} (SrGaSiH) > C_{ij} (BaGaSiH). This ordering indicates that CaGaSiH is the most rigid and least compressible among the three compounds, followed by SrGaSiH and BaGaSiH.

The elastic constant C_{11} is notably the highest compared to other constants, reflecting a significant resistance to changes in shape and volume along the directions associated with C_{11}. This high value implies that these compounds exhibit substantial resistance to deformations in the directions involving changes in length and volume. This resistance is due to the high packing density in these directions, where atoms are tightly packed, making deformation more challenging.

Conversely, the compounds show greater compressibility along the c-axis compared to the a-axis. This is evident from the smaller value of the elastic constant C_{33} relative to C_{11}. The larger value of C_{11} compared to C_{33} indicates that the compounds are more resistant to deformation in the a-direction than in the *c*-direction. Essentially, the material is stiffer and less prone to compression along the a-axis, while it is more compressible along the c-axis.

Additionally, the comparison between C_{44} and C_{66} reveals that shear deformation is more easily achieved in the (001) plane compared to the (100) plane. The smaller value of C_{44} suggests that shear deformation within the (001) plane requires less energy compared to shear deformation in the (100) plane, where C_{66} is larger. This implies that the material exhibits greater shear resistance along the (100) plane, making it less deformable in this direction.

These insights into the elastic constants provide a deeper understanding of the mechanical properties of XGaSiH compounds, highlighting their varying degrees of rigidity, compressibility, and shear resistance. This information is crucial for evaluating the materials' performance and stability in practical applications, particularly in scenarios where mechanical properties play a significant role.

The melting points and bulk modulus can be used to predict the hydrogen decomposition temperatures in XGaSiH materials. The hydrogen decomposition temperatures for these materials (X = Si, Ca, or Ba) can be estimated using their melting points. The equation $T_m = 607 + 9.3 \times B$ where T_m is expressed in K, and B is expressed in GPa [41], indicates the relationship between the melting temperatures and the bulk modulus. This equation shows that the melting temperature depends on the bulk modulus, which is an indicator of the strength of the crystal bonds in the material. The results indicate a similar relationship to that found by Fine between elastic constants and melting points for metals and non-metallic materials [42]. The melting points of the compounds are as follows: CaGaSiH (T_m = 1240.95 K) > BaGaSiH (T_m = 1185.85 K) > SrGaSiH (T_m = 1176.45 K). The bulk modulus order for the compounds is CaGaSiH (B = 68.16 GPa) > BaGaSiH (B = 62.24 GPa) > SrGaSiH (B = 61.23 GPa). Based on this order of melting points and bulk modulus, BaGaSiH is expected to decompose at a lower temperature than CaGaSiH and SrGaSiH.

The shear modulus G and bulk modulus B were calculated using the Hill model [43,44], which averages the results from the Voigt model [45] and the Reuss model [46]. Specifically, for hexagonal systems, we determined the following values: The Voigt shear modulus (G_v), the Voigt bulk modulus (B_v), the Reuss shear modulus (G_R), the Reuss bulk modulus (B_R), as well as the Hill shear modulus (G_H) and the Hill bulk modulus (B_H).

$$B_V = \frac{2C_{11} + 2C_{12} + 4C_{13} + C_{33}}{9} \tag{19}$$

$$B_R = \frac{(C_{11} + C_{12})C_{33} - 2C_{13}^2}{C_{11} + C_{12} - 4C_{13} + 2C_{33}} \tag{20}$$

$$G_V = \frac{4C_{11} + 2C_{33} - 4C_{13} - 2C_{12} + 12C_{44} + 6C_{66}}{30} \tag{21}$$

$$G_R = 15\left(\frac{4C_{11} + 4C_{12} + 8C_{13} + 2C_{33}}{(C_{11} + C_{12})C_{33} - 2C_{13}^2} + \frac{6}{C_{11} - C_{12}} + \frac{6}{C_{44}} + \frac{3}{C_{66}}\right)^{-1} \tag{22}$$

$$B_H = \frac{1}{2}(B_V + B_R) \tag{23}$$

$$G_H = \frac{1}{2}(G_V + G_R) \tag{24}$$

The Voigt and Reuss models are foundational approaches used to understand and characterize the elastic behavior of composite materials. Each model offers a distinct perspective based on different assumptions about the material's internal structure and response to applied stresses. The Voigt Model operates under the assumption of material homogeneity. This model presumes that the composite material behaves as if it were a single, uniform substance with consistent elastic properties throughout. In other words, it treats the material as though all its phases are perfectly aligned and share the same mechanical response to stress. This approach is often used to estimate the upper bound of the material's elastic moduli, reflecting the maximum stiffness and resistance to deformation that the composite could exhibit if it were uniformly stressed. The Reuss Model, on the other hand, adopts a different perspective by considering the composite material as an aggregate of distinct phases, each with its own specific elastic properties. According to this model, the composite is viewed as a collection of separate materials, each contributing to the overall mechanical behavior in a way that reflects their individual characteristics. The Reuss model provides an estimate of the lower bound of the material's elastic moduli, representing the minimum stiffness and deformation resistance of the composite when accounting for the variations in phase properties.

Together, these models offer a range of elastic moduli for the composite material—Voigt providing an upper bound and Reuss providing a lower bound. However, real-world composites often exhibit elastic behaviors that lie between these extremes due to the complex interactions and distributions of different phases within the material.

To address this intermediate behavior, the Hill Model is frequently employed. The Hill model combines the assumptions of both the Voigt and Reuss models by averaging the upper and lower bounds obtained from each approach. This method provides a more balanced estimate of the composite's elastic properties, reflecting a more realistic scenario where the material's response to stress is neither perfectly homogeneous nor entirely phase-separated. By integrating the Voigt and Reuss predictions, the Hill model offers a practical means to estimate the effective elastic moduli of composite materials in a way that accounts for both the idealized extremes.

These models provide theoretical bounds for the bulk and shear

moduli of composite materials, with the Voigt model offering upper limits and the Reuss model providing lower limits. In practice, however, the behavior of real composite materials often falls between these extremes. To address this, the Hill model is utilized. The Hill model combines the predictions of both the Voigt and Reuss models by averaging their results. This approach accounts for the constraints imposed by both extreme cases and provides a more realistic estimate of the overall elastic properties of composite materials.

The Hill model effectively integrates the Voigt model's assumption of homogeneity with the Reuss model's consideration of heterogeneous phases, offering a balanced perspective. It calculates the average elastic properties, which are useful for understanding the material's overall behavior. This model is instrumental in deriving the bulk modulus (B_H) and shear modulus (G_H), as outlined in Equations (23) and (24), respectively. By averaging the Voigt and Reuss estimates, the Hill model provides a practical method for evaluating the effective elastic properties of composite materials. The equations used to compute the Young's modulus E and the Poisson's ratio σ are as follows [47]:

$$\begin{cases} E = \dfrac{9\,B\,G}{(G + 3B)} \\ \sigma = \dfrac{3B - 2G}{2(3B + G)} = \dfrac{1}{2}\left(1 - \dfrac{E}{3B}\right) \end{cases} \tag{25}$$

Research findings reported in Ref. [48] demonstrate that XGaSiH materials (where X represents Sr, Ca, and Ba) exhibit notably high compressibility. This characteristic indicates that these materials are able to undergo substantial compression when subjected to applied stress. The study also reveals that the elastic moduli of XGaSiH materials, including Young's modulus and bulk modulus, are significantly lower compared to those typically observed in common metals [49] and intermetallic compounds [50].

This lower elastic modulus suggests that XGaSiH materials are less resistant to deformation under stress, which is consistent with their high compressibility. Despite their lower modulus values, these materials share a common high compressibility property, making them unique in their mechanical behavior.

These insights are important for assessing the suitability of XGaSiH materials for various applications, particularly in hydrogen storage systems. In such applications, materials must possess both compressive strength and flexibility to effectively manage and contain hydrogen. The high compressibility of XGaSiH materials suggests they can accommodate significant deformation, which could be beneficial in contexts where material flexibility and adaptability are critical. Pugh proposed that the ratio of the bulk modulus to the shear modulus can be used to determine the ductility of a material and its ability to deform under stress without breaking [51]. The shear modulus reflects the material's resistance to deformation when a large force is applied, while the bulk modulus indicates the material's resistance to fracture. The compound CaGaSiH has a higher bulk modulus than BaGaSiH and SrGaSiH. For example, B_V(CaGaSiH) = 74.73 GPa > B_V(SrGaSiH) = 66.43 GPa > B_V(BaGaSiH) = 63.87 GPa, indicating that CaGaSiH has stronger bonding compared to SrGaSiH and BaGaSiH (see Table 6).

Regarding the B/G ratio, if this ratio is higher than 1.75, it means the material has high ductility and can withstand deformation without breaking. All the studied XGaSiH exhibit brittleness, meaning their B/G ratio is less than 1.75, and therefore, they tend to fracture rather than deform under stress.

Young's modulus E is a measure of material hardness, determining its resistance to deformation under uniaxial stress or compression. When force is applied to a material, Young's modulus measures the relationship between stress (applied force) and strain (change in length).

In transitioning from CaGaSiH to SrGaSiH and then to BaGaSiH, a consistent decrease in material hardness is observed. This means that as we move from Ca to Sr and then to Ba, the materials become less hard. This trend is evident in Table 6 where E_H (CaGaSiH) = 135.43 GPa, E_H (SrGaSiH) = 130.87 GPa, and E_H (BaGaSiH) = 123.80 GPa. CaGaSiH exhibits greater resistance to deformation under pressure and tension compared to SrGaSiH and BaGaSiH. This indicates that CaGaSiH is harder and less prone to deformation under stress or tension than the other materials.

Table 6
Modules of elasticity for XGaSiH (X = Sr, Ca, Ba) using GGA.

	SrGaSiH	CaGaSiH	BaGaSiH
B_V (GPa)	66.435	74.733	63.874
B_R (GPa)	61.232	68.167	62.242
B_H (GPa)	63.833	71.450	63.058
G_V (GPa)	57.782	58.738	53.596
G_R(GPa)	55.209	55.639	51.969
G_H (GPa)	56.495	57.188	52.782
E_V (GPa)	134.385	139.631	125.645
E_R (GPa)	127.351	131.216	121.962
E_H (GPa)	130.874	135.431	123.803
σ_V	0.162	0.185	0.172
σ_R	0.153	0.175	0.173
σ_H	0.158	0.180	0.172
B_H/G_H	1.129	1.249	1.194
A_B %	4.075	4.594	3.294
A_G %	2.277	2.709	1.541
A^u	0.317	0.374	0.182

When a material undergoes uniaxial deformation, Poisson's ratio σ determines how its volume changes. When σ is less than 0.5, the material does not experience a permanent volume change during elastic deformation, meaning it returns to its original state after the load is removed. For XGaSiH (X = Sr, Ca, or Ba), a significant volume change during deformation has been observed due to the low σ values. The σ_H value for BaGaSiH is 0.172, for SrGaSiH it is 0.158, and these values are lower than the σ_H value for CaGaSiH, which is 0.180. This indicates that BaGaSiH and SrGaSiH undergo more noticeable volume changes during deformation.Poisson's ratio σ is very important as it provides insight into the bonding forces within the material [52]. In solids with central forces that attract particles towards their center, the minimum value for σ is 0.25 and the maximum is 0.5 [53]. The calculated σ values for XGaSiH show that they have strong central bonding since their σ values fall within this range. Comparing the bulk modulus values obtained from C_{ij} (elastic constants) and those derived from the equation of state (EOS) using the GGA approximation, we find a good agreement. This agreement confirms the accuracy of the C_{ij} calculations as the B values obtained from both C_{ij} and EOS match.

Thermal conductivity experiments can be employed to anticipate phase transitions [54]. The Debye model is predicated on a direct connection between thermal conductivity coefficients and specific heat, that can be determined by utilizing the Debye temperature. The Debye temperature [47] is intricately connected to a variety of physical properties of materials, including melting points, elastic constants, and specific heat. Vibrational excitation at low temperatures is primarily driven by acoustic vibrations. The Debye temperature can be estimated by employing elastic constants rather than determining the low-temperature specific heat. The Debye temperature θ_D is found by calculating the average sound velocity, v_m, which is derived by calculating the longitudinal v_l and transverse v_t elastic wave velocities. In order to determine the variables of XGaSiH (X = Sr, Ca, or Ba) at zero pressure, the GGA method was implemented. Table 7 illustrates these figures. Compared to transverse elastic shear waves, longitudinal elastic

Table 7
Longitudinal, transversal, and average sound velocity values (v_l,v_t, v_m in m/s), temperature of Debye (θ_D in K) for XGaSiH (X = Sr, Ca, Ba) using GGA.

Compounds	ν_t (m/s)	ν_l (m/s)	ν_m (m/s)	θ_D(K)
SrGaSiH	3637.65	5709.17	3998.62	453.17
CaGaSiH	4050.51	6509.51	4464.17	521.62
BaGaSiH	3265.41	5191.93	3594.70	395.56

compression waves propagate at a faster rate. The average sound velocity, v_m, can be used to calculate the Debye temperature (θ_D) as follows [55]:

$$\theta_D = \frac{h}{K_B}\left(\frac{3n}{4\pi}\left(\frac{N_a\,\rho}{M}\right)\right)^{\frac{1}{3}} \nu_m \tag{26}$$

Equation (27) [52] provides the average sound velocity of the polycrystalline material, where h is Planck's constant, k_B is Boltzmann's constant, n is the number of atoms in the unit cell, N_A is Avogadro's number, ρ is the density, and M is the molecular weight of the solid.

$$\nu_m = \left[\frac{1}{3}\left(\frac{2}{V_t^3} + \frac{1}{V_l^3}\right)\right]^{-\frac{1}{3}} \tag{27}$$

The shear modulus and bulk modulus from Navier's equation (28) [52] are employed to determine the longitudinal v_l and transverse ν_t sound velocities.

$$\nu_t = \sqrt{\frac{G}{\rho}} \text{ and } \nu_l = \sqrt{\frac{B + 4/3}{\rho} G} \tag{28}$$

Based on the results obtained, it is clear that the theoretical Debye temperature of CaGaSiH(521.62 K) is higher compared to compounds SrGaSiH (453.17 K)and BaGaSiH (395.56 K), indicating increased resistance relative to XGaSiH (where X = Sr or Ba). This discrepancy in temperatures also implies that the fracture toughness of CaGaSiH is greater than that of SrGaSiH and BaGaSiH. In solids, θ_D serves as an indicator of atomic bond strength, with its higher values pointing to strong bonds between CaGaSiH and BaGaSiH, as well as similar compounds. Research indicates that θ_D shows an inverse correlation with molecular weight and functions as a measure of covalent bond strength in materials [56]. We observe consistency between the calculated θ_D values derived from elastic constants (C_{ij}) and those estimated using the Gibbs2 code, and these calculated values are in the hydrogen storage properties section using equation (17). This alignment strengthens our confidence in the accuracy of the obtained results.

The elasticity variations within crystals have a substantial impact on a variety of physical processes, such as heterogeneous plastic deformation, fracture behavior, and elastic instability. However, in order to improve the mechanical flexibility of structural hydrides in mobile applications, such as hydrogen storage, it is imperative to calculate their elastic variability [47]. One approach to assessing this variability is to calculate heterogeneous shear moduli, which are used to measure the extent of property differences in atomic bonds across different levels. Equations can be employed to express these parameters for hexagonal materials [57].

$$A_1 = 4C_{44} / (C_{11} + C_{33} - 2C_{13}) \tag{29}$$

$$A_2 = 2C_{66} / (C_{11} - C_{12}) \tag{30}$$

The shear anisotropy factors, denoted as A_1 for the {100} plane and A_2 for the {001} plane, are detailed in Table 5. Elastic anisotropy is indicated by deviations of these factors from unity. Specifically, for SrGaSiH, BaGaSiH, and CaGaSiH using the GGA approximation, the values of A_1 are approximately 0.97, 0.85, and 1.10, respectively. Conversely, A_2 is consistently equal to 1 across all three compounds, indicating isotropic shear modulus within the {001} plane. This suggests significant shear anisotropy in XGaSiH compounds within the {100} plane compared to isotropic behavior in the {001} plane for the compounds studied.

The second method entails the calculation of the percentage of elastic anisotropy in compression (A_B) and shear (A_G), as defined in Ref. [57]:

$$A_B = (B_V - B_R) / (B_V + B_R) \times 100 \tag{31}$$

$$A_G = (G_V - G_R) / (G_V + G_R) \times 100 \tag{32}$$

The elastic anisotropy is quantified as follows: The elastic properties of a material are quantified by AB and A_G in relation to various directions. A_B contrasts the bulk moduli calculated using the Voigt and Reuss models, thereby revealing the anisotropy of the material's bulk modulus. In the same vein, A_G compares the shear moduli derived from these models, which indicates the anisotropy of the material's shear modulus. These measures aid in comprehending the material's intrinsic anisotropic behavior, which is a result of its crystal structure and microstructural configuration.

Anisotropy in bulk and shear moduli arises from directional variations in stiffness resulting from the presence of preferred bonding directions or crystal orientations. For instance, in anisotropic materials, the stiffness and compliance vary depending on the crystallographic directions due to the uneven distribution of atomic bonds or variations in the crystal lattice. A_B and A_G provide critical insights into the extent and nature of these deviations from isotropy, offering a valuable understanding of the material's mechanical behavior and its response to applied forces. Such insights are crucial for predicting how the material will perform under different stress conditions and for designing applications where directional properties are significant [47].

The bulk modulus, which quantifies a material's resistance to uniform compression, often reflects isotropic behavior in homogeneous materials. However, in anisotropic materials, the bulk modulus can vary depending on the direction of applied pressure due to the directional dependence of stiffness. This anisotropy is often influenced by the material's microstructural organization and crystalline structure, such as the alignment of grain boundaries, the presence of defects, or the orientation of crystal axes.

Understanding the anisotropy of both bulk and shear moduli is essential for predicting and optimizing material performance in practical applications. Materials with significant anisotropy may exhibit pronounced differences in mechanical responses when subjected to stress in various directions, which can impact their performance in structural applications, load-bearing components, or any scenario where directional mechanical properties are critical. Additionally, the effects of anisotropy extend to other material properties, including thermal and electrical conductivities, which are influenced by the material's elastic behavior. Therefore, a comprehensive understanding of elastic anisotropy not only aids in assessing mechanical properties but also helps in tailoring materials to achieve desired performance characteristics in a wide range of engineering and technological applications. These directional variations lead to distinct responses to volume changes under stress along different crystallographic axes, resulting in different bulk modulus values. This anisotropic behavior reflects the material's internal structural alignment and bonding configurations, crucial for understanding its mechanical properties in diverse loading conditions and applications.

The values of A_B and A_G for compounds reflect their elasticity variations: zero values indicate uniform elasticity in all directions, while high values ($A_B = A_G = 100\%$) indicate significant elasticity differences among directions, affecting material properties and applications. Table 6 results using the GGA method show variance rates for volume and shear variance for XGaSiH compounds (where X = Sr, Ca, Ba). A_B rates for SrGaSiH, CaGaSiH, and BaGaSiH are approximately 4.0754%, 4.5948%, and 3.2940%, respectively. A_G rates for SrGaSiH, CaGaSiH, and BaGaSiH are about 2.2771%, 2.7094%, and 1.5412%, respectively. These compounds exhibit moderate variance in shear and volume moduli under pressure conditions. Additionally, CaGaSiH shows significantly varied shear and volume moduli compared to SrGaSiH and BaGaSiH, suggesting CaGaSiH may be more influenced by crystalline directions and microscopic arrangements in materials.

The universal index in the third method is calculated by Ref. [57]:

$$A^U = 5\frac{G_V}{G_R} + \frac{B_V}{B_R} - 6 \tag{33}$$

A^U measures the degree of elasticity anisotropy in materials: $A^U = 0$ indicates isotropic elasticity, while non-zero A^U values indicate anisotropic elasticity. According to data from Table 6, using the GGA method, AU values are approximately 0.3179, 0.3748, and 0.1827 for SrGaSiH, CaGaSiH, and BaGaSiH respectively. These values signify significant directional variations in elasticity across the materials. Elastic anisotropy is primarily influenced by variations in bulk and shear moduli [58].

The research mentioned is insufficient in depth to precisely determine the elastic characteristics of crystals. Existing studies may not fully capture the nuanced variations in elastic properties across different crystallographic directions, leaving gaps in understanding the complete elastic behavior of materials. To address these limitations, it is recommended to incorporate additional metrics, such as linear compressibility and the inverse of Young's modulus, when evaluating elastic properties, particularly for surface structures.

Linear compressibility provides insight into the material's response to pressure along different crystallographic directions, reflecting how the material's volume changes under uniform compression. This measure is particularly useful for understanding the anisotropic nature of materials, as it can reveal variations in compressibility that are directionally dependent. Similarly, the inverse of Young's modulus—often referred to as the compliance—can provide additional clarity regarding how materials deform under applied stresses in different orientations. These metrics offer complementary perspectives to the bulk and shear moduli, helping to build a more comprehensive picture of the material's elastic behavior.

Hexagonal systems, in particular, exhibit varying linear compressibility profiles depending on the crystallographic orientation. In hexagonal crystals, the elastic properties can differ significantly along different axes due to the inherent anisotropy of the hexagonal lattice structure. For example, the compressibility may be greater along one axis compared to another, reflecting the directional dependence of the material's stiffness. This orientation-dependent behavior underscores the importance of considering multiple directions when evaluating elastic properties.

Incorporating these additional metrics and acknowledging the orientation-dependent nature of hexagonal systems can lead to more accurate and detailed assessments of elastic characteristics. This approach allows for a better understanding of how materials will behave in real-world applications, where directional properties and surface interactions play a crucial role in determining performance and stability. By addressing these aspects, researchers and engineers can optimize material selection and design for applications requiring precise control over mechanical properties.

$$B = (S_{11} + S_{12} + S_{13}) - n_2^3(S_{11} + S_{12} - S_{13} - S_{33}) \tag{34}$$

Equation (34) describes B, which is the linear compressibility, detailing how materials respond to volume changes due to applied stress. B is linked to components of the compliance tensor, S_{ij}, and the direction n_3. S_{ij} represents the elastic constants related to deformability, while n_1, n_2, and n_3 are directional cosines corresponding to the x, y, and z axes in spherical coordinates. The relationship between S_{ij} and the elastic constants C_{ij} describes how these deformability constants influence and are influenced by the elastic constants C_{ij},in the hexagonal system S_{ij} equations are written as follows [59]:

$$\begin{cases} S_{11} = 1/C_{11} \\ S_{33} = 1/C_{33} \\ S_{12} = S_{21} = -C_{12}/(C_{11}C_{22}) \\ S_{13} = S_{31} = -C_{13}/(C_{11}C_{33}) \\ S_{44} = 1/C_{44} \end{cases} \tag{35}$$

The directional dependence of Young's modulus for a hexagonal crystal along the direction of the unit vector n_i, can be determined by the following equation [60]:

$$E = \frac{1}{(1-n_3^2)^2 S_{11} + n_3^4 S_{33} + n_3^2(1-n_3^2)(2S_{13} + S_{44})} \tag{36}$$

The equation for Young's modulus in the hexagonal structure is essential for assessing a material's resistance to deformations caused by mechanical pressures and for comprehending its behavioral traits. This equation is dependent on the compliance tensor and directional parameters.

Fig. 12 displays the computed linear compressibility values for the XGaSiH compounds (X = Sr, Ca, and Ba) based on their theoretical elastic constants. Linear compressibility refers to how much a material compresses under applied stress in a specific direction. The values are represented in a three-dimensional surface plot, where the distance from the coordinate center to the surface indicates the magnitude of linear compressibility in that direction.

In isotropic materials, linear compressibility is uniform in all directions, resulting in a spherical representation of compressibility in such cases. However, the absence of spherical forms in Fig. 12 indicates that the XGaSiH compounds exhibit non-isotropic linear compressibility, meaning their compressibility varies with direction. Specifically, the (XY) plane shows a lower variation in elastic properties compared to the (X = Y), (XZ), and (YZ) planes. This observation suggests that while compressibility in the (XY) plane exhibits isotropic characteristics (uniform in all directions within the plane), the other planes experience varying degrees of compressibility depending on their orientation.

Fig. 13 presents the Young's modulus tensor components for SrGaSiH, CaGaSiH, and BaGaSiH compounds, derived from elastic compliance constants. Young's modulus measures a material's stiffness and is direction-dependent in anisotropic materials. The figure illustrates a closed three-dimensional surface representing Young's modulus tensor components originating from a specific direction. In materials exhibiting full symmetry, this surface would be spherical.

For the XGaSiH compounds, which are orthorhombic, the surface appears nearly spherical, indicating minimal asymmetry in their elastic response. This near-spherical shape suggests that while there is some degree of anisotropy, it is relatively small. Elastic anisotropy is more pronounced on the (X = Y), (XZ), and (YZ) surfaces compared to the (XY) surface. On the (XY) surface, the Young's modulus tensor component shows isotropic behavior, meaning its stiffness is consistent in all directions within this plane.

These observations provide a detailed understanding of how XGaSiH materials respond to applied stresses and strains in different directions. The non-isotropic nature of their linear compressibility and the near-isotropic Young's modulus behavior highlight their directional dependencies and potential applications where specific mechanical responses are required.

The elastic properties of XGaSiH compounds, such as C_{11}, C_{33}, and C_{44}, are crucial in determining the effectiveness of these materials in hydrogen storage applications. These properties are directly related to the material's ability to withstand mechanical stresses and changes that occur during hydrogen absorption and desorption. Values of the elastic properties for compounds like CaGaSiH, SrGaSiH, and BaGaSiH illustrate how they handle deformations caused by hydrogen pressures. For example, XGaSiH compounds with high elasticity and positive elastic moduli are better able to withstand stresses without failure, meaning they can absorb larger amounts of hydrogen while maintaining structural stability.

The high flexibility of these materials allows them to expand and contract under hydrogen pressure without losing their structural integrity. Materials with good elastic properties can return to their original shape after pressure is removed, enhancing their stability and effectiveness as hydrogen storage materials. High elasticity also means that the material can handle the stresses associated with absorbed hydrogen,

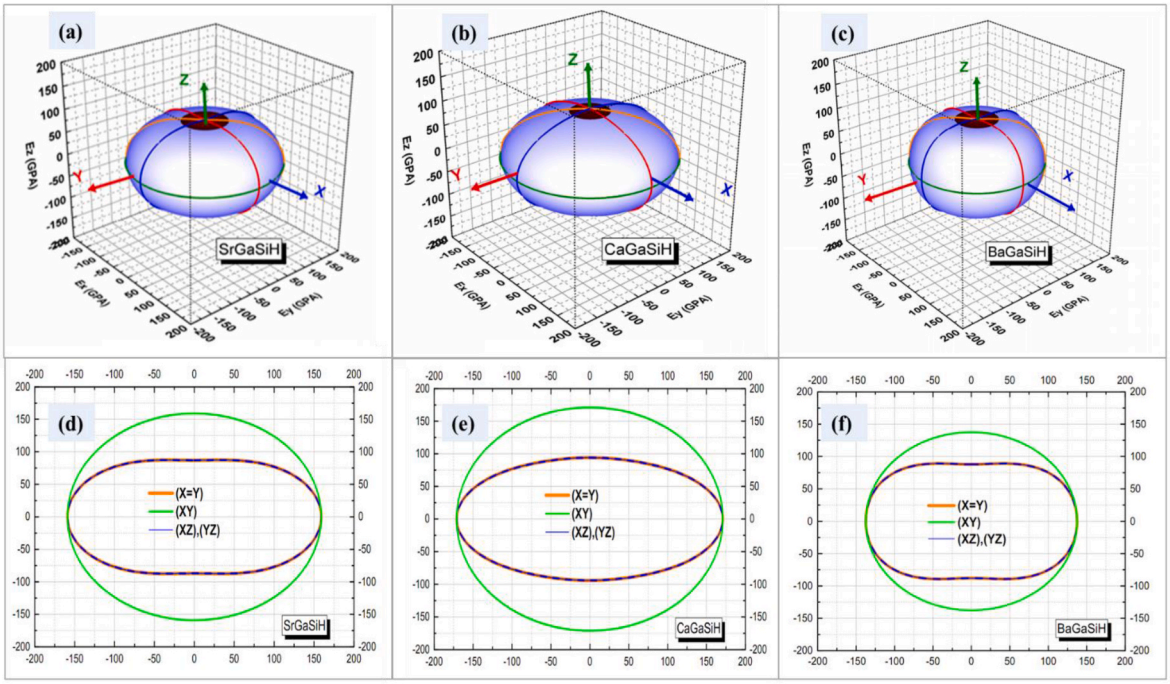

Fig. 12. **(a), (b)** and **(c)** represent the 3D surface of the Young's modulus for SrGaSiH, CaGaSiH and BaGaSiH, **(d),(e)** and **(f)** their cross sections in different planes respectively.

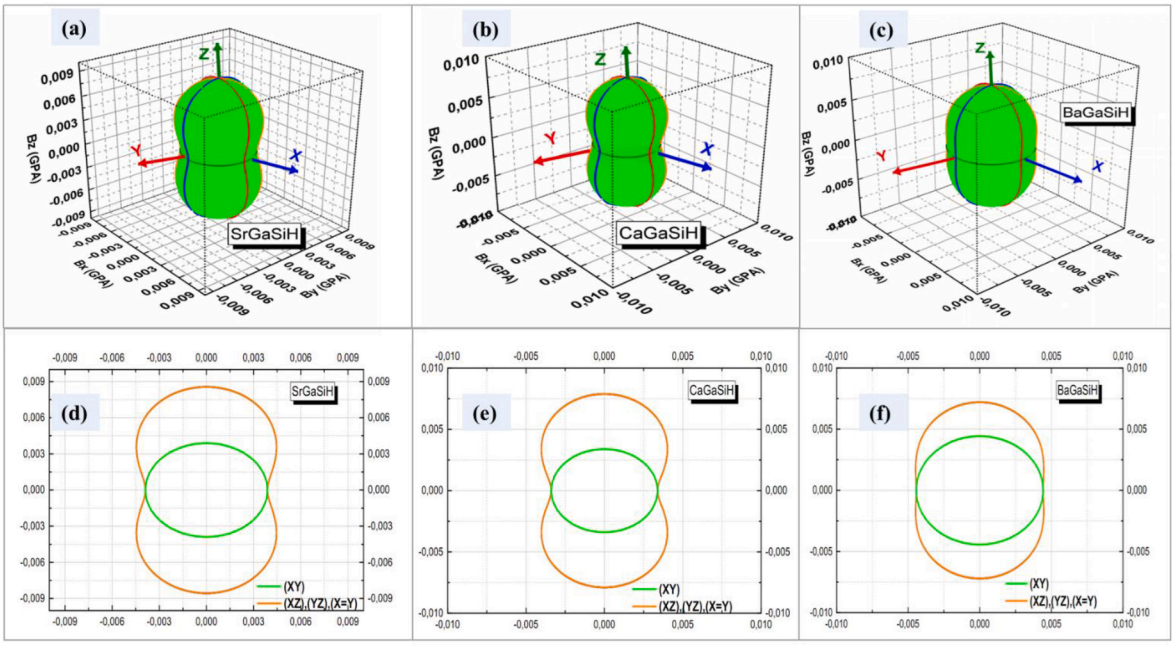

Fig. 13. (a), (b) and (c) represent the orientation-dependent linear compressibility for SrGaSiH, CaGaSiH and BaGaSiH, respectively. **(d), (e)** and **(f)** represent linear compressibility projections in different planes for SrGaSiH, CaGaSiH and BaGaSiH respectively.

reducing the likelihood of cracks or structural failures. Studying the elastic properties is particularly important because it affects the material's ability to store hydrogen safely and efficiently. Materials with high flexibility will perform better in storing larger amounts of hydrogen, making them more suitable for future energy applications. Additionally, good elastic properties help mitigate damage caused by changes in operational conditions, making the material more reliable and effective in industrial applications.

Based on the elastic properties of XGaSiH compounds, such as deformation strengths and elasticity, their ability to provide reliable and sustainable performance in hydrogen storage applications can be predicted. These properties contribute to understanding how materials respond to environmental and mechanical changes, thereby enhancing their capability to meet future hydrogen storage requirements.

4. Conclusion

Our study delivers a thorough examination of the structural,

electronic, thermodynamic, and mechanical properties of XGaSiH compounds (where X = Sr, Ca, Ba), revealing significant insights into their potential for hydrogen storage applications.

Structural Properties: The XGaSiH compounds exhibit a robust hexagonal arrangement of Ga and Si layers, which is crucial for their hydrogen storage capabilities. This stable structural configuration allows the materials to absorb and release hydrogen effectively at appropriate temperatures. The resilience of these materials under various conditions ensures reliable hydrogen cycling without degradation, positioning them as promising candidates for practical hydrogen storage systems where durability is essential.

Electronic Properties: Analysis using GGA, LDA, mBJ-GGA, and mBJ-LDA methods shows that these compounds have band gaps ranging from 0.1 eV to 0.9 eV, indicating significant conductivity potential. The proximity of these bands to the Fermi level enhances electronic interactions, which are critical for efficient hydrogen adsorption and release. This electronic behavior underlines the suitability of these materials for applications requiring high electronic performance, such as semiconductor devices.

Thermodynamic Properties: Our study reveals considerable volume expansion of XGaSiH compounds under heating, with detailed analyses of heat capacity, thermal conductivity, thermal expansion, and the Grüneisen parameter. These properties indicate that the materials maintain their structural integrity despite thermal fluctuations, making them suitable for environments with variable temperatures. Their high thermal stability ensures effective operation in diverse conditions, which is crucial for reliable hydrogen storage.

Mechanical Properties: Anisotropy analysis indicates significant differences in shear modulus between the {100} and {001} planes, affecting the materials' ability to handle mechanical stresses during hydrogen cycling. Specifically, CaGaSiH shows the highest compressibility, followed by SrGaSiH and BaGaSiH. The ability of these materials to accommodate volumetric changes without compromising structural integrity is essential for long-term hydrogen storage applications.

Implications and Future Research: The combination of high compressibility, notable conductivity potential, and robust thermal stability makes XGaSiH compounds valuable for renewable energy applications, especially in developing efficient hydrogen storage solutions. Future research should focus on enhancing these materials through structural modifications or doping to improve hydrogen storage capacity and electrical conductivity. Additionally, studying their behavior under varying environmental conditions and exploring their scalability for industrial applications will be crucial for advancing their practical use in renewable energy technologies.

CRediT authorship contribution statement

H. Ammi: Writing – review & editing, Writing – original draft, Software, Conceptualization. **Z. Charifi:** Writing – review & editing, Writing – original draft, Supervision, Data curation. **H. Baaziz:** Software, Methodology, Investigation, Conceptualization. **T. Ghellab:** Writing – original draft, Resources, Conceptualization. **L. Bouhdjer:** Validation, Methodology, Data curation. **S. Adalla:** Methodology, Investigation, Formal analysis, Data curation. **H.Y. Ocak:** Software, Formal analysis, Data curation, Conceptualization. **Ş. Uğur:** Software, Investigation, Data curation. **G. Uğur:** Methodology, Data curation, Conceptualization.

Declaration of competing interest

The authors declare that they have no known competing financial interests or personal relationships that could have appeared to influence the work reported in this paper.

Acknowledgments

The authors (H. Ammi, T. Ghellab, Z. Charifi and H. Baaziz) would like to thank the general directorate for scientific research and technological development for their financial support during the realization of this work.

References

[1] Barbir F. PEM electrolysis for production of hydrogen from renewable energy sources. Sol Energy 2005;78(5):661–9.
[2] Turner JA. A realizable renewable energy future. Science 1999;285(5428):687–9.
[3] Xu X, Dong Y, Hu Q, Si N, Zhang C. Electrochemical hydrogen storage materials: state-of-the-art and future perspectives. Energy Fuel 2024;38(9):7579–613.
[4] Azeem W, Shahzad MK, Wong YH, Tahir MB. Ab-initio calculations for the study of the hydrogen storage properties of CsXH3 (X= Co, Zn) perovskite-type hydrides. Int J Hydrogen Energy 2024;50:305–13.
[5] Chen LQ, Zhao Y. From classical thermodynamics to phase-field method. Prog Mater Sci 2022;124:100868.
[6] Wang M, Jiang C, Zhang S, Song X, Tang Y, Cheng HM. Reversible calcium alloying enables a practical room-temperature rechargeable calcium-ion battery with a high discharge voltage. Nat Chem 2018;10(6):667–72.
[7] Cheng S, Cheng X, Tahir MH, Wang Z, Zhang J. Synthesis of rice husk activated carbon by fermentation osmotic activation method for hydrogen storage at room temperature. Int J Hydrogen Energy 2024;62:443–50.
[8] Fang S, Li J, Zou K, Shuai H, Xu L, Deng W, Ji X. Zintl chemistry: current status and future perspectives. Chem Eng J 2022;433:133841.
[9] Kauzlarich SM. Zintl phases: from curiosities to impactful materials. Chem Mater 2023;35(18):7355–62.
[10] Hoffmann P. Tomorrow's energy: hydrogen, fuel cells, and the prospects for a cleaner planet. 2006.
[11] Xu N, Chen Y, Chen S, Zhang W, Li S, Song R, Zhang J. First-principles investigations for the hydrogen storage properties of XVH3 (X= Na, K, Rb, Cs) perovskite type hydrides. J Mater Res Technol 2023;26:4825–48.
[12] Song R, Xu N, Chen Y, Chen S, Zhang J, Li S, Zhang W. Exploring the structural, physical and hydrogen storage properties of Cr-based perovskites YCrH3 (Y= Ca, Sr, Ba) for hydrogen storage applications. Ceram Int 2024.
[13] Brehm JA. Predicted bulk photovoltaic effect in hydrogenated Zintl compounds. J Mater Chem C 2018;6(6):1470–5.
[14] Tran F. WIEN2k: an augmented plane wave plus local orbitals program for calculating crystal properties. 2018.
[15] Perdew JP, Burke K, Ernzerhof M. Phys Rev Lett 1996;77:3865.
[16] Otero-de-la-Roza A, Abbasi-Pérez D, Luaña V. Comput Phys Commun 2011;182:2232.
[17] Otero-de-la-Roza A, Luaña V. Comput Phys Commun 2011;182:1708.
[18] Blanco MA, Francisco E, Luaña V. Comput Phys Commun 2004;158:57.
[19] Girifalco LA. Oxfort university press. 2000. p. 62.
[20] Jamal M, Bilal M, Ahmad I, Jalali-Asadabadi S. IRelast package. J Alloys Compd 2018;735:569–79.
[21] Lee MH, Björling T, Hauback BC, Utsumi T, Moser D, Bull D, Häussermann U. Crystal structure, electronic structure, and vibrational properties of M AlSiH (M= Ca, Sr, Ba): hydrogenation-induced semiconductors from the AlB 2-ty. 2008.
[22] Evans MJ, Holland GP, Garcia-Garcia FJ, Häussermann U. Polyanionic gallium hydrides from AlB2-type precursors AeGaE (Ae= Ca, Sr, Ba; E= Si, Ge, Sn). J Am Chem Soc 2008;130(36):12139–47.
[23] Björling T, Noréus D, Jansson K, Andersson M, Leonova E, Edén M, Häussermann U. SrAlSiH: a polyanionic semiconductor hydride. Angew Chem Int Ed 2005;44(44):7269–73.
[24] Lu Y, Tada T, Toda Y, Ueda S, Wu J, Li J, Hosono H. Interlayer states arising from anionic electrons in the honeycomb-lattice-based compounds A e AlSi (A e= Ca, Sr, Ba). Phys Rev B 2017;95(12):125117.
[25] Kranak VF, Evans MJ, Daemen LL, Pro en T, Lee MH, Sankey OF, U. Haussermann. Solid State Sci 2009;11:1847.
[26] Vajeeston P, Fjellvåg H. Revised electronic structure, Raman and IR studies of AB 2 H 2 and ABC H (A= Sr, Ba; B= Al, Ga; C= Si, Ge) phases. RSC Adv 2014;4(1):22–31.
[27] Murnaghan FD. The compressibility of media under extreme pressures. Proc Natl Acad Sci USA 1944;30(9):244–7.
[28] Evans MJ, Holland GP, Garcia-Garcia FJ, Häussermann U. Polyanionic gallium hydrides from AlB2-type precursors AeGaE (Ae= Ca, Sr, Ba; E= Si, Ge, Sn). J Am Chem Soc 2008;130(36):12139–47.
[29] Austin J. Supporting information for the manuscript. 2009. p. 1–42.
[30] Gingl F, Vogt T, Akiba E. J Alloys Compd 2000;306:127.
[31] Wagner FR, Baranov AI, Grin Y, Kohout M. A position-space view on chemical bonding in metal diborides with AlB2 type of crystal structure. Z Anorg Allg Chem 2013;639(11):2025–35.
[32] Ammi H, Charifi Z, Baaziz H, Ghellab T, Bouhdjer L, Adalla S. Electronic, elastic, and thermodynamic properties of complex hydrides XAlSiH (X= Sr, Ca, and Ba) intended for hydrogen storage: an ab-initio study. Phys Scripta 2024;99(6).
[33] Evans MJ, Lee MH, Holland GP, Daemen LL, Sankey OF, Häussermann U. Vibrational properties of the gallium monohydrides SrGaGeH, BaGaSiH, BaGaGeH, and BaGaSnH. J Solid State Chem 2009;182(8):2068–73.
[34] Häussermann U. Z Kristallogr 2008;223:628.

[35] Elton DC. The origin of the Debye relaxation in liquid water and fitting the high frequency excess response. Phys Chem Chem Phys 2017;19(28):18739–49.
[36] Pluengphon P, Tsuppayakorn-aek P, Sukmas W, Inceesungvorn B, Bovornratanaraks T. Dynamical stabilization and H-vacancy diffusion kinetics of lightweight complex hydrides: ab initio study for hydrogen storage improvement. Int J 2021.
[37] Barieau RE. The correct application of the Gibbs—Helmholtz equation to reversible galvanic cells in which several phases are in equilibrium at one of the electrodes. J Am Chem Soc 1950;72(9):4023–6.
[38] Berube V, Chen G, Dresselhaus MS. Impact of nanostructuring on the enthalpy of formation of metal hydrides. Int J Hydrogen Energy 2008;33(15):4122–31.
[39] Radovic M, Lara-Curzio E, Riester L. Comparison of different experimental techniques for determination of elastic properties of solids. Mater Sci Eng, A 2004; 368(1–2):56–70.
[40] Mouhat F, Coudert FX. Necessary and sufficient elastic stability conditions in various crystal systems. Phys Rev B 2014;90(22):224104.
[41] Özer T. Study of first principles on anisotropy and elastic constants of YAl3 compound. Can J Phys 2020;98(4):357–63.
[42] Ghellab T, Charifi Z, Baaziz H, Latteli H, Güler M, Uğur ŞULE, Uğur GÖKAY. The elastic, mechanical, and thermodynamic properties of NaXH4 (X= B, Al) intended for the storage of hydrogen: an ab-initio study. Physica 2022.
[43] Hill R. The elastic behaviour of a crystalline aggregate. Proc Phys Soc 1952;65(5): 349.
[44] Hill R. New derivation of some elastic extremum principles. Progress in applied mechanics, The Prager anniversary 1963;ume:99–106.
[45] Voigt W. Lehrbuch der Kristallphysik (Textbook of crystal physics). Leipzig und Berlin: BG Teubner; 1928.
[46] Reuss A. Calculation of the flow limits of mixed crystals on the basis of the plasticity of monocrystals. Z Angew Math Mech 1929;9(1):49–58.
[47] Ravindran P, Fast L, Korzhavyi PA, Johansson B, Wills J, Eriksson O. Density functional theory for calculation of elastic properties of orthorhombic crystals: application to TiSi 2. J Appl Phys 1998;84(9):4891–904.
[48] Caputo R, Tekin A. Ab-initio crystal structure prediction. A case study: NaBH4. J Solid State Chem 2011;184(7):1622–30.
[49] Wills JM, Eriksson O, Söderlind P, Boring AM. Trends of the elastic constants of cubic transition metals. Phys Rev Lett 1992;68(18):2802.
[50] Nakamura M. In: Westbrook JH, Fleischer RL, editors. Intermetallic compounds: principles, vol. 1. New York: Wiley; 1994. p. 873.
[51] Pugh SF. XCII. Relations between the elastic moduli and the plastic properties of polycrystalline pure metals. London, Edinburgh Dublin Phil Mag J Sci 1954;45 (367):823–43.
[52] Anderson OL. A simplified method for calculating the Debye temperature from elastic constants. J Phys Chem Solid 1963;24(7):909–17.
[53] Rusman NAA, Dahari M. A review on the current progress of metal hydrides material for solid-state hydrogen storage applications. Int J Hydrogen Energy 2016;41(28):12108–26.
[54] Gross KJ, Thomas GJ, Jensen CM. Catalyzed alanates for hydrogen storage. J Alloys Compd 2002;330:683–90.
[55] Gariboldi E, Colombo LP, Fagiani D, Li Z. Methods to characterize effective thermal conductivity, diffusivity and thermal response in different classes of composite phase change materials. Materials 2019;12(16):2552.
[56] Shi YJ, Du YL, Chen G. First-principles study on the elastic and electronic properties of hexagonal ε-Fe3N. Comput Mater Sci 2013;67:341–5.
[57] Panda KB, Chandran KR. Determination of elastic constants of titanium diboride (TiB2) from first principles using FLAPW implementation of the density functional theory. Comput Mater Sci 2006;35(2):134–50.
[58] Ranganathan SI, Ostoja-Starzewski M. Universal elastic anisotropy index. Phys Rev Lett 2008;101(5):055504.
[59] Hearmon RFS. The elastic constants of anisotropic materials—II. Adv Phys 1956;5 (19):323–82.
[60] Nye JF. Physical properties of crystals: their representation by tensors and matrices. Oxford university press; 1985.
[61] Lee MH, Sankey OF, Björling T, Moser D, Noréus D, Parker SF, Häussermann U. Vibrational properties of polyanionic hydrides SrAl2H2 and SrAlSiH: new insights into Al− H bonding interactions. Inorg Chem 2007;46(17). 6987-69.
[62] Björling T, Noréus D, Jansson K, Andersson M, Leonova E, Edén M, Häussermann U. SrAlSiH: a polyanionic semiconductor hydride. Angew Chem Int Ed 2005;44(44):7269–73.